science.sciencemag.org/content/368/6496/1265/suppl/DC1

Supplementary Materials for

Very fast CRISPR on demand

Yang Liu*, Roger S. Zou*, Shuaixin He, Yuta Nihongaki, Xiaoguang Li, Shiva Razavi, Bin Wu†, Taekjip Ha†

*These authors contributed equally to this work.
†Corresponding author. E-mail: tjha@jhu.edu (T.H.); bwu20@jhu.edu (B.W.)

Published 12 June 2020, *Science* **368**, 1265 (2020)
DOI: 10.1126/science.aay8204

This PDF file includes:

Materials and Methods
Supplementary Text
Figs. S1 to S26
Tables S1 to S9
Caption for Table S10
Captions for Movie S1 to S3
References

Other Supplementary Material for this manuscript includes the following:
(available at science.sciencemag.org/content/368/6496/1265/suppl/DC1)

MDAR Reproducibility Checklist
Table S10
Movies S1 to S3

Materials and methods

Cas9 purification

BL21-CodonPlus (DE3)-RIL competent cells (Agilent Technologies 230245) were transformed with Cas9 plasmid (Addgene #67881) and inoculated in 5 ml of LB-ampicillin media. The bacteria culture was first allowed to grow overnight (37 °C, 220 rpm) and then transferred to 1 L of LB supplemented with ampicillin and 0.1 % glucose until OD_{600} of ~0.5. Subsequently, the cells were induced with IPTG at a final concentration of 0.2 mM and maintained overnight at 18 °C. The bacteria cells were pelleted at 4500 x g, 4 °C for 15 min and resuspended in 20 ml of lysis buffer containing 20 mM Tris pH 8.0, 250 mM KCl, 20 mM imidazole, 10% glycerol, 1 mM TCEP, 1 mM PMSF, and cOmplete™ EDTA-free protease inhibitor tablet (Sigma-Aldrich 11836170001). This cell suspension was lysed using a microfluidizer and the supernatant containing Cas9 protein was clarified by spinning down cell debris at 16,000 x g, 4 °C for 40 min and filtering with 0.2 µm syringe filters (Thermo Scientific™ F25006). Ni-NTA agarose bead slurry (Qiagen 30210) was pre-equilibrated with 5 column volumes of lysis buffer. The clarified supernatant was then loaded at 4 °C. The protein-bound Ni-NTA beads were washed with 15 column volumes wash buffer containing 20 mM Tris pH 8.0, 800 mM KCl, 20 mM imidazole, 10% glycerol, and 1 mM TCEP. Gradient elution was performed with buffer containing 20 mM HEPES pH 8.0, 500 mM KCl, 10% glycerol, and varying concentrations of imidazole (100, 150, 200, and 250 mM) at 7 ml collection volume per fraction. The eluted fractions were tested on an SDS-PAGE gel and imaged by Coomassie blue (Biorad 1610400) staining. To remove any DNA contamination, 1 ml Q Sepharose® column (GE Healthcare 17051005) was charged with 1M KCl and then equilibrated with elution buffer containing 250 mM imidazole. The purified protein solution was then passed over the Q column at 4 °C. The flow-through was collected and dialyzed in a 10 kDa SnakeSkin™ dialysis tubing (Thermo Fisher Scientific 68100) against 2 L of 20 mM HEPES pH 7.5, and 500 mM KCl, 20% glycerol at 4 °C, overnight. Next day, the protein was dialyzed for an additional 3 hours in fresh dialysis buffer. The final Cas9 protein was concentrated to 10 µg/µl using Amicon® Ultra 10 kDa centrifugal filter unit (Millipore UFC801024), aliquoted, and flash-frozen and stored at -80 °C.

In vitro cleavage assay and Electrophoretic Mobility Shift Assay (EMSA)

All guide RNA sequences are in Table S1. All synthetic template DNA sequences are in Table 2. 10 µM cr:tracr cgRNA solution was prepared at equal molar ratio by heating to 95 °C for 5 min and cooling on heat block for 1 hour. 3 pmol of Cas9 was incubated with 5 pmol of cgRNA to form RNP for 30 min in 10 µl of 1x NEBuffer 3.1 (New England Biolabs). 60 fmol of target DNA was added and thoroughly mixed before placing the tube on 37 °C heat block for 1 min.

For *in vitro* cleavage kinetics measurements, 365 nm light was applied for time t = min(T, 30 sec), where T is the total incubation time of 1 sec, 5 sec, 10 sec, 30 sec, 1 min, 2 min, 5 min, 10 min, 20 min, 30 min. A no light control was allowed to incubate in 37 °C for 30 min. Immediately after time T, the reaction was quenched in 95 °C for 10 min. To evaluate light dosage effect, 365 nm light was applied for 1 sec, 5 sec, 10 sec, 30 sec, 1 min, 2 min before incubation at 37 °C for 30 min. After incubation, 10 µg of Proteinase K (Thermo Fisher) was added to each tube and further incubated in 55 °C for 15 min. The DNA was then purified with QIAquick PCR Purification Kit (Qiagen) before loading on an agarose gel for visualization.

For EMSA, a tube was incubated at 37 °C for 30 min and directly loaded on an agarose gel.

4% E-Gel EX Agarose Gels run on an E-Gel iBase™ Power System (Thermo Fisher) were used for all *in vitro* experiments. To calculate cleavage efficiency, the integrated intensity of cleaved bands was divided by that of total DNA as quantified using ImageJ.

Cell culture

Human embryonic kidney 293 cell line (HEK293T) and human U-2 osteosarcoma cell line (U-2 OS) were cultured at 37 °C under 5 % CO_2 in Dulbecco's Modified Eagle's Medium (DMEM, Corning), supplemented with 10 % FBS (Corning), 100units/ml penicillin and 100µg/ml streptomycin (DMEM complete). Cells were tested every month for mycoplasma.

Electroporation of Cas9 RNP

All guide RNA sequences are in Table S1. To anneal cr:tracr cgRNA, equal volumes of 100 µM cgRNA (Bio-Synthesis Inc) with tracrRNA (Integrated DNA Technologies) were mixed and heated to 95 °C for 5 min in a thermocycler. The mixture was allowed to cool on benchtop for 5 min. To form RNP complex, 10 µg/µl of purified Cas9 was mixed with 50 µM cr:tracr cgRNA at a ratio of 1:1.2, which was then incubated for additional 20 min at room temperature. Cells were properly maintained to a confluency of ~90 % prior to electroporation. Cells were then trypsinized and centrifuged in DMEM and 1x PBS sequentially (3min, 200g). Supernatant was discarded and 20 µl of nucleofection solution (Lonza) was mixed thoroughly with cell pellet, prior to the addition of 5 µl RNP solution. 1 µl of Cas9 Electroporation Enhancer (Integrated DNA Technologies) was also included. Electroporation was performed according to the manufacturer's instructions on the 4D-Nucleofector™ Core Unit (Lonza). SF Cell Line 4D-Nucleofector™ X Kit S with code CA-189 was used for HEK293T cells. SE Cell Line 4D-Nucleofector™ X Kit S with code DN-100 was used for U-2 OS cells. DMEM complete was added before plating to culture wells.

Preparing samples for CRISPR-Cas9 kinetics measurements in cells

HEK 293T cells were introduced with Cas9 RNP through electroporation, plated to 96-wells, and incubated in standard cell culture conditions. 12 h after electroporation, cells were exposed to a flashlight that delivered 1.3 J/cm^2 of 365nm wavelength light. Cells were harvested at different time points by removal of media and washing with 200 µl/well ice-cold DPBS. Cells were subsequently placed on ice before they were transferred to -80 °C. To harvest genomic DNA from cells, cells were immediately taken out of -80°C and placed in 95 °C heat block for 5 min. Samples were transferred to ice and genomic DNA was isolated using PureLink™ Genomic DNA Mini Kit (Thermo Fisher Scientific K182001) according to the manufacturer's instructions, except with 1 h (instead of 10 min) incubation with lysis buffer/Proteinase K/RNase A at 55 °C.

Droplet digital PCR assay for measuring double-strand break frequencies

ddPCR protocol is adapted from previous literature (*17*). Oligo sequences for library preparation are in Table S3. Two amplicons were designed for each locus of interest. One amplicon (target1) includes the Cas9 cleavage site; the other (target2) is a nearby sequence that is not cleaved. One dual-quenched qPCR probe (IDT) was designed for each amplicon. Primers and probes were designed using guidelines by Bio-Rad (http://www.bio-rad.com/en-us/applications-technologies/planning-droplet-digital-pcr-experiments?ID=MDV33OKG4). 10-50 ng of purified genomic DNA were added to a 20 µl reaction with final probe concentration of 900 nM and final

primer concentration of 250 nM. For all four loci tested (*ACTB*, *IFT88*, *MYC*, *PPP1R2*), BamHI-HF (New England BioLabs) were added to the reaction mixture to ensure better separation of signals during amplification. Droplets were created using Droplet Generation Oil for Probes, DG8 Gaskets, DG8 Cartridges, and QX200 Droplet Generator (Bio-Rad); PCR amplification was performed using ddPCR Supermix for Probes (no dUTP) (Bio-Rad). Droplets were transferred to a 96-well PCR plate and heat-sealed using PX1 PCR Plate Sealer (Bio-Rad). PCR amplification was performed with the following conditions: 95 °C for 10 min, 40 cycles of {94 °C for 30 sec, variable annealing temperatures for 30 sec, 72 °C for 2 min}, 98 °C for 10 min, 12 °C hold. Annealing temperatures for *ACTB*, *IFT88*, *MYC*, and *PPP1R2* were 60 °C, 56 °C, 54 °C, and 58 °C respectively. Following PCR, droplets were individually scanned by the QX200 Droplet Digital PCR system (Bio-Rad). Droplets plotted in each fluorescent channel (FAM/HEX) were all well separated in clusters, and a threshold was set to bin droplets to positive and negative labels.

To generate standard curves, DNA harvested from wild-type HEK293T cells was cleaved using restriction enzymes (Fig. S4). Restriction enzymes were selected to only cleave within target1, and not target2. EcoRV-HF was used for *ACTB*, SfcI was used for *IFT88* and *MYC*, and EagI-HF was used for *PPP1R2* (New England BioLabs) according to manufacturer's instructions. Cleaved and non-cleaved DNA samples were mixed at ratios of 1:0, 2:1, 1:1, 1:2, 1:4, 1:10, 1:100, 0:1. ddPCR was performed on the samples with the same protocol as Cas9 cleavage samples. Duplicates were obtained for each locus and linear regression was calculated using all data points.

Double-strand break (DSB) frequency was calculated using the following formula: [target1−,target2+]/([target1−,target2+] + [target1+,target2+]), where target1− indicates negative droplets for the target1 amplicon, target2+ indicates positive droplets for the target2 amplicon.

Sanger Sequencing for measuring insertions or deletions

PCR primer sequences are in Table S4. Genomic DNA samples were amplified with PCR using Q5 Hot Start High-Fidelity 2X Master Mix (New England BioLabs M0494). PCR amplification was performed with the following conditions for *ACTB*, *MYC*, and *PPP1R2*: 98 °C for 30 sec, 35 cycles of {98 °C for 10 sec, 71 °C(*ACTB*)/67 °C(*MYC*)/68 °C(*PPP1R2*) for 10 sec, 72 °C for 20 sec}, 72 °C for 2 min, and 4 °C hold. For *IFT88*: 98 °C for 30 sec, 35 cycles of {98 °C for 10 sec, 60 °C for 20 sec, 65 °C for 40 sec}, 65 °C for 5 min, and 4 °C hold. After PCR, cleanup was performed using QiaQuick PCR Purification Kit (Qiagen 28104) following the manufacturer's instructions. 3 ng/µl of each sample was submitted to Genewiz for Sanger sequencing. Indels were calculated using TIDE analysis at https://tide.deskgen.com/.

Next generation amplicon sequencing for measuring insertions or deletions

Oligo sequences for library preparation are in Table S5 and S6. Genomic DNA samples were amplified with PCR using Q5 Hot Start High-Fidelity 2X Master Mix (New England BioLabs M0494). PCR amplification as performed with the following conditions: 98 °C for 30 sec, 31 cycles (*ACTB*), 33 cycles (*MYC* and *IFT88*), or 32 cycles (*PPP1R2*) of {98 °C for 10 sec, 71 °C(*ACTB*)/65 °C(*MYC*)/58 °C(*IFT88*)/68 °C(*PPP1R2*) for 10 sec, 72 °C for 20 sec}, 72 °C for 5 min, and 4 °C hold. After amplicon PCR, cleanup was performed using 1.6x AMPure XP (Beckman Coulter A63881) following the manufacturer's instructions. Dual-indexing PCR was performed using KAPA HiFi HotStart ReadyMix (Roche 07958935001) with the following conditions: 95 °C for 3 min, 10 cycles of {95 °C for 30 sec, 55 °C for 30 sec, 72 °C for 30 sec},

72 °C for 5 min, and 4 °C hold. PCR cleanup was performed using 1x AMPure XP; samples were pooled, diluted, and loaded onto a MiSeq (Illumina). Sequencing was performed with the following number of cycles "151 | 8 | 8 | 151" with the paired-end Nextera sequencing protocol. Sequencing reads were either demultiplexed automatically using MiSeq Reporter (Illumina) or with a custom Python script to individual FASTQ files. For indel calling, sequencing reads were scanned for exact matches to two 20-bp sequences that flank +/-20 bp from the ends of the target sequence. If no exact matches were found, the read was excluded from analysis. After additional filtering for an average quality score > 20, an indel is defined as a sequence that differs in length from the reference length.

Normalized Indels calculation from raw Indel % and DSB %

Raw Indel % is obtained from either TIDE analysis of Sanger sequencing or deep amplicon sequencing. DSB % is obtained from DSB-ddPCR. We define Normalized Indel % to be the Indel % from all DNA at a particular locus, not just from PCR-amplifiable DNA. This factors in cleaved DNA that cannot be PCR amplified for indel measurements. Norm. Indel % = Indel % × (100 – DSB %) / 100. The sum of DSB %, Normalized Indel % and Intact % equals 100%.

GUIDE-seq

HEK293T cells were electroporated with the protocol described previously, with an additional 25 pmol dsODN mixed with the RNP. 72 h after electroporation, cells were harvested with DPBS and genomic DNA was isolated using DNeasy Blood & Tissue Kit (Qiagen 69506) according to the manufacturer's instructions, except with 1 h (instead of 10 min) incubation with lysis buffer/Proteinase K at 55 °C. Library preparation was performed according to the original protocol with corrected adaptor sequences (*19*). The library was quantified with qPCR using NEBNext® Library Quant Kit for Illumina® (New England BioLabs E7630), pooled, diluted, and loaded onto a MiSeq (Illumina) using the Nano Reagent Kit v2. Sequencing was performed with the following number of cycles: "150 | 8 | 16 | 150". Data analysis was done using code adapted from https://github.com/aryeelab/guideseq, with the original filter for sequences containing six or fewer mismatches between candidate off-target sites and the on-target sequence including the NGG PAM.

Chromatin immunoprecipitation (6 samples per experiment)

Electroporation was performed on a larger scale than in the section titled "Electroporation of Cas9 RNP" with the following changes: 6 µl of 100 uM of crRNA was annealed to 6 µl of 100 uM tracrRNA; 147.6 µl SF solution + 32.4 µl supplement were used totaling 180 µl of the electroporation solution; 4 µl of electroporation enhancer was used; after mixing with cells, the final volume was approximately 260 µl, split equally between two 100 µl cuvettes. After electroporation, the cells were split to 6 samples corresponding to no-light and time points (2 min, 5 min, 15 min, 30 min, 1 h) after Cas9 activation.

The ChIP protocol was adapted from previous literature (*18*). Briefly, cells were washed once with room temperature PBS, then washed off the plate with 10 ml DMEM and transferred to 15 ml falcon tubes. 721 µl of 16 % formaldehyde (methanol free) was added for 15 min in RT. 750 µl of 2M glycine was added to quench the formaldehyde. Cells were spun down with 1200g at 4 °C for 3 min, then washed with ice-cold PBS twice, spinning down with the same centrifugation conditions. Cells were then resuspended in 4ml lysis buffer LB1 (50mM HEPES, 140mM NaCl,

1mM EDTA, 10% glycerol, 0.5% Igepal CA-630, 0.25% Triton X-100, pH to 7.5 using KOH, add 1x protease inhibitor right before use) for 10 min at 4 °C, then spun down 2000g with at 4 °C for 3 min. The supernatant was decanted. Cells were then resuspended in 4ml LB2 (10mM Tris-HCl pH 8, 200mM NaCl, 1mM EDTA, 0.5mM EGTA, pH to 8.0 using HCl, add 1x protease inhibitor right before use) for 5 min at 4 °C, spun down with the same protocol, and the supernatant decanted. Cells were then resuspended in 1.5 ml LB3 (10mM Tris-HCl pH 8, 100mM NaCl, 1mM EDTA, 0.5mM EGTA, 0.1% Na-Deoxycholate, 0.5% N-lauroylsarcosine, pH to 8.0 using HCl, add 1x protease inhibitor right before use) and transferred to 2 ml Eppendorf tubes for sonication with 50 % amplitude, 30 s ON, 30 s OFF for 8 min total time (Fisher 150E Sonic Dismembrator). Samples were spun down with 20000g at 4 °C for 10 min, and supernatant was transferred to 1.5 ml LB3 + 300 µl of 10 % Triton X-100 in a 15 ml falcon tube.

Beads pre-loaded with antibodies were prepared before cell harvesting. 75 µl Protein A beads (Thermo Fisher) were used per IP. 450 µl beads (for 6 IPs) were transferred to 2 ml Eppendorf tube on magnetic stand. Beads were washed twice with blocking buffer BB (0.5% BSA in PBS), then resuspended in 900 µl BB (150 µl per IP). 18 µl of antibody (3 µl per IP) (MRE11 – Novus NB100-142; γH2AX – Abcam ab81299) were added and placed on rotator for 1-2 h. Right before IP, the 2 ml tube was placed on a magnetic rack and washed 3x with BB, before resuspending in 600 µl BB. 100 µl of beads in BB were transferred to each IP and placed in 4 °C rotator for 6+ hours.

Samples were transferred to 2 ml Eppendorf tubes on a magnetic stand, washed 6x with 1 ml RIPA buffer (50 mM HEPES, 500 mM LiCl, 1 mM EDTA, 1 % Igepal CA-630, 0.7 % Na-Deoxycholate, pH to 7.5 using KOH), then washed 1x with 1 ml TBE buffer (20 mM Tris-HCl pH 7.5, 150 mM NaCl), before decanting. Beads containing ChIP-ed DNA were mixed with 70 µl elution buffer EB (TODO) and incubated 65 °C for 6+ hours. 40 µl of TE buffer was mixed to dilute the SDS, followed by 2 µl of 20 mg/ml RNaseA (New England BioLabs) for 30 min at 37 °C. 4 µl of 20 mg/ml Proteinase K (New England BioLabs) was added and incubated for 1 h at 55 °C. The genomic DNA was column purified (Qiagen) and eluted in 41 µl nuclease free water.

High-throughput sequencing and data processing of ChIP samples

Oligo sequences for library preparation are in Table S7. End-repair/A-tailing was performed on 17 µl of ChIPed DNA using NEBNext® Ultra™ II End Repair/dA-Tailing Module (New England BioLabs), followed by ligation (MNase_F/MNase_R) with T4 DNA Ligase (New England BioLabs). 11 and 13 cycles of PCR using PE_i5 and PE_i7XX primer pairs were performed for γH2AX and MRE11 ChIP samples, respectively to amplify libraries. Samples were pooled, quantified with QuBit (Thermo), Bioanalyzer (Agilent) and qPCR (BioRad), then sequenced on a NextSeq 500 (Illumina) using high-output paired 2x36bp reads. All ChIP-seq raw reads in FASTQ format and processed alignments in BAM format are uploaded to Sequence Read Archive (SRA) under BioProject accession PRJNA609749 (https://www.ncbi.nlm.nih.gov/bioproject/PRJNA609749).

Reads were demultiplexed after sequencing using bcl2fastq. Paired-end reads were aligned to hg38 using bowtie2. Samtools was used to filtered for mapping quality >= 25, remove singleton reads, convert to BAM format, remove potential PCR duplicates, index reads, count the number of mapped reads, and subset to normalize for mapped reads after filtering steps. The software that

performs these steps as well as all subsequent analyses (fragment analysis, binning analysis) are open source on GitHub (https://github.com/rogerzou/chipseq_cgRNA).

Fragment analysis from paired-end ChIP-seq reads

A fragment is defined by two aligned and correctly oriented paired-end reads. Fragments can be categorized into two sub-populations: (1) Fragments that "span" the DSB site, defined to be those that cross the Cas9 target site, implying that this DNA fragment was not broken at the Cas9 target site at the time of cell fixation, and (2) Fragments that "end at" the DSB site, defined to be fragments that start or end from a 10 bp window centered at the DSB site and attributed to unrepaired DSBs (*18*). Peak are represented as "fragment pileups", which incorporate the entire inferred DNA fragment, i.e. the middle part of each DNA strand that is not sequenced is counted. Fragments per million is therefore defined as the number of relevant fragments divided by the total number of fragments in the sequencing sample.

γH2AX MACS2 peak calling and binning analysis

MACS2 (https://github.com/taoliu/MACS) was used to detect the 'main peak', using the following settings: --broad --broad-cutoff 0.05 --min-length 5000 --max-gap 100000. The width of the contiguous broadPeak that spanned the cleavage site was recorded as the 'main peak'.

For total enrichment, custom python code was used to bin read counts every 50 kb, with 1 kb sub-bins (50 sub-bins per bin). For all time points after Cas9 activation, students t-test ($p < 0.05$, paired, one-sided, with Bonferroni correction) was used to test for significant increase in read counts above no-light control. The width of total enrichment was determined as the longest sequence of bins with read counts significantly higher than no-light and gaps less than 2 megabases long.

Plasmid and retroviral transduction

To clone the Cas9-EGFP plasmid, we replaced the dCas9-EGFP plasmid (Addgene # 51023) with an active Cas9 component. For viral production, GP2-293 packaging cells were used and cultured on a 10 cm dish for overnight. Next day, 23 µg of transfer vector, 5 µg of pVSVg and 5 µg of pGag-Pol plasmids were transfected into the packaging cells using polyethylenimine (PEI). 8-12 h after transfection, the medium containing PEI was discarded and the cell culture was gently replenished with 15 ml of fresh DMEM medium. 48 h after transfection, 15 ml of virus was harvested and purified through a 0.45 µm filter.

Construction of Stable U-2 OS cell lines

To make stable U-2 OS cell lines expressing Cas9-EGFP, we infected WT U-2 OS cells with Cas9-EGFP retrovirus and enriched positive cells with puromycin selection for a week. Subsequently, a monoclonal cell line was selected with only 2 copies of Chromosome 3 and low expression of Cas9-EGFP. To introduce mCherry-53BP1, the Cas9-EGFP cells were further infected with mCherry-BP1 retrovirus (Addgene #19835) and cultured for a week. Finally, the cells expressing both Cas9-EGFP and mCherry-BP1 were selected by FACS.

Transient transfection of cgRNA

To deliver cgRNA into living U-2 OS cells, we transiently transfected 15 pmol of pre-annealed cr:tracr cgRNA to one 6-well imaging dish using Lipofectamine RNAiMAX Transfection Reagent (Thermo Fisher Scientific). After 24 h incubation, Cas9-EGFP foci were easily detectable using

epi-fluorescence microscopy. To target the repetitive region, we transfected the cells with 15 pmol of Ch3 cgRNA. To target single cleavage site, we transfected the cells with a mixture of 5 pmol of Ch3 (truncated 11mer) targeting the repetitive region and ~ 10 pmol of cgRNA targeting *PPP1R2*.

Immunofluorescence microscopy

U-2 OS cells stably expressing Cas9-EGFP cells were seeded onto glass coverslip and transfected with specific gRNAs for 12-24 h. After light stimulation, cell fixation was performed with 4 % of paraformaldehyde in 1x PBS for 10 min and then quenched by 1x PBS supplemented with 0.1 M glycine for 10 min. After thoroughly rinsing with 1x PBS, 0.5 % Triton-X was used to permeabilize cell membrane for 10 min. 2 % w/v BSA in 1x PBS was used to passivate the sample for 1 h and at room temperature. Without further rinsing, primary antibody was diluted in 1x PBS and directly added into the chamber for targeting the protein of interests. After 1 h incubation, primary antibody was removed and the sample was thoroughly washed with 1x PBS three times. Secondary antibody was typically diluted in 1:1000 and applied to the sample for 1 h. Finally, the sample was rinsed three times and mounted with Prolong Diamond mounting media (Thermo Fisher Scientific) overnight.

Alexa647 and Alexa750 conjugated Goat anti-rabbit IgG (H+L) antibody (A21245, A21039) and Cy5 conjugated Goat anti-mouse antibody (A10524) were purchased from Thermo Fisher. Anti-MDC1 (Ab11169) and anti-Phospho-DNA-PKcs (S2056) (Ab124918) antibodies were purchased from Abcam (Cambridge, MA). Anti-53BP1 (NB100-304), anti-γH2AX (NB100-384) and anti-MRE11 (NB100-473) were purchased from Novus Biologicals (Centennial, CO). Anti-Phospho-ATM (Ser1981) monoclonal antibody (10H11) (MA1-2020) was purchased from Thermo Fisher. Dilution of primary antibody was based on the recommended ratio from the manufacturers.

Single particle fluorescence imaging of living cells

U-2 OS cells stably expressing Cas9-EGFP and 53BP1-mCherry were seeded onto glass coverslip and transfected with cgRNA for 24 h. To activate Cas9/cgRNA, we illuminated the cell sample with either custom 365 nm LED (30 s) or 405 nm laser (10 s) before imaging. We used Nikon Ti-E fluorescence microscope equipped with two Andor EMCCDs for simultaneous imaging of Cas9 foci and 53BP1-mCherry foci, which were excited by 488 nm and 561 nm lasers, respectively. All live cell imaging experiments were performed at 37 °C and in L-15 media supplemented with 10 % FBS and 1 % Penicillin/Streptomycin.

Image analysis

To analyze the time-course of 53BP1 recruitment to DSB, we first used ‘u-track’ single-particle tracking program developed by Danuser lab (*29*) (https://www.utsouthwestern.edu/labs/danuser/software/) to track the centroid of Ch3Rep loci marked by Cas9-EGFP. We defined a square region of interest in the 53BP1-mCh channel centered on the genomic locus. The fluorescence intensities of 53BP1-mCherry foci were measured in the cropped square image using a Gaussian fit. The fluorescence of the whole nucleus was measured and fit to an exponential curve. The 53Bp1-mCherry foci intensities were divided by the fitted exponential curve to correct photobleaching.

To quantify the colocalization fraction between Ch3Rep and endogenous foci (Fig. S16), 3D image datasets were processed into 2D datasets in FIJI using maximum intensity projection. We calibrated the pixel shift between GFP and Cy5 channels using 100nm TetraSpeck beads and registered them with a custom-built MATLAB (MathWorks) package. After registration, colocalization between Ch3Rep and repair proteins was further analyzed with a custom-built CellProfiler3 pipeline (*30*). Two masks representing either Ch3Rep loci or repair protein foci were first created. For each Ch3Rep locus, a "colozalization" event was counted if its mask overlaps with the repair protein mask. To calculate the colocalization ratio, we divided the number of Ch3Rep loci that colocalized with repair proteins by the total number of Ch3Rep loci.

Immunoblotting

Cells were lysed in RIPA buffer, pelleted by centrifugation, and resuspended in SDS sample buffer. 50-100 μg of isolated protein samples were loaded on Tris·HCl polyacrylamide gels (Criterion, Bio-Rad), and were then transferred onto a polyvinylidene fluoride membrane. The membranes were blocked with in a 1:1 solution of TBST and Odyssey blocking buffer for 1 h and then were incubated with primary antibodies in 5% BSA in TBST overnight at 4°C. Then, specific fluorescent conjugated secondary antibody was applied and prepared for imaging as per manufacturer's protocol (LI-COR Biosciences). Blots were then imaged on a LI-COR Odyssey CLx at high resolution. The primary antibodies used in the studies were: Anti–phospho- Chk2 (Thr68) antibody (2661T) (Cell Signaling Technology, Danvers, MA, USA); Anti-Actin C4 Antibody (MAB1501) (Cell Signaling); Anti–Phospho-ATM (Ser1981) Monoclonal Antibody (10H11) (Invitrogen); Anti-Phospho-DNA PKcs (S2056) antibody (ab124918)(Abcam); Anti-Phospho-rH2A: (2577S) (Cell Signaling).

Spatial control of Cas9 activation at single allele

To induce DSBs at a repetitive locus (Ch3Rep) specifically to a targeted allele, U2OS cells stably expressing Cas9-EGFP and 53BP1-mCherry were transfected with cgRNA targeting Ch3Rep. 12 h later, a focused laser (405 nm, 78 nW) was used to apply transient light stimulation exclusively to a 1.5×1.5 μm square containing one Cas9-EGFP focus for a period of 10 s.

To induce a single DSB at PPP1R2 specifically to a targeted allele, U2OS cells stably expressing Cas9-EGFP and 53BP1-mCherry were transfected with both truncated sgRNA targeting Ch3Rep and cgRNA targeting PPP1R2 locus. 24 h later, a focused laser (405 nm, 65 μW) was used to apply transient light stimulation exclusively to a 1.5×1.5 μm square containing one Cas9-EGFP focus for a period of 100 ms.

After light stimulation, fluorescence microscopy was immediately started to track the formation of 53BP1-mCherry foci.

Supplementary Text

Theory and modeling

1. Kinetic model of Cas9-induced DSB and indel formation

We adapted a previously described kinetic model of DSB and indel formation (*21*). Assume at the time of uncaging, there is a fraction of DNA foci B_0 are pre-bound by Cas9/cgRNA. Because cleavage by pre-bound Cas9/cgRNA occurs within seconds of light illumination (t=0) and the earliest data points for DSB and indels are at 30 s, we assign DSB at time 0 equal to the pre-bound fraction ($\mathrm{DSB}(t=0) = B_0$). An intact DNA target that is not bound by an RNP is cut with an apparent cleavage rate k_s to generate DSB. Note that the rate k_s depends on the DNA locus and activated Cas9-gRNA concentration, and it is mainly determined by the rate of target searching which is much slower than cleavage. A DSB can be repaired perfectly with a rate k_p, or it can be repaired with a rate k_m to generate an indel.

Based on these definitions, we established the Model I assuming that indels cannot be re-cut by Cas9:

$$\mathrm{Intact} \underset{k_p}{\overset{k_s}{\rightleftharpoons}} \mathrm{DSB} \overset{k_m}{\rightharpoonup} \mathrm{Indel} \qquad \text{(Model I)}$$

Because the active pool of Cas9/cgRNA from the one-time delivery is expected to degrade over time, the proportion of active pool is modeled with an exponential decay function

$$Cas_t = \exp(-k_{deg}\, t) \qquad (1)$$

where k_{deg} is the rate of removal of Cas9/cgRNA from the active pool (Cas9/cgRNA that is able to act on the genomic DNA substrate).

This reaction is then modeled as a set of coupled ordinary differential equations:

$$\frac{d\,\mathrm{DSB}}{dt} = k_s\, Cas_t\, \mathrm{Intact} - (k_m + k_p)\,\mathrm{DSB}, \qquad (2)$$

$$\frac{d\,\mathrm{Indel}}{dt} = k_m\,\mathrm{DSB}, \qquad (3)$$

satisfying the normalization condition

$$\mathrm{Intact} + \mathrm{DSB} + \mathrm{Indel} = 1 \qquad (4)$$

and the initial condition:

$$\mathrm{Intact}(0) = 1 - B_0, \qquad \mathrm{DSB}(0) = B_0, \quad \mathrm{Indel}(0) = 0\,. \qquad (5)$$

An alternative model is that the indel can be re-cut with the rate k_{rc}. Because there are many different types of indels generated by repair, the rate k_{rc} should be taken as an average of different indels. In general, k_{rc} is expected to be 0 or much smaller than the wide type rate k_s. In addition, because of the insertion and deletion, the position of indel-generated DSB will be different from the original one. These indel-generated DSBs could be repaired perfectly or produce other indels, but it is unlikely to regenerate the original DNA sequence. This Model II is summarized by the reaction scheme:

$$\mathrm{Intact} \underset{k_p}{\overset{k_s}{\rightleftharpoons}} \mathrm{DSB}_1 \overset{k_m}{\rightharpoonup} \mathrm{Indel} \underset{k_m+k_p}{\overset{k_{rc}}{\rightleftharpoons}} \mathrm{DSB}_2. \qquad \text{(Model II)}$$

The differential equations to describe Model II are

$$\frac{d\,\mathrm{DSB}_1}{dt} = k_s\, Cas_t\, \mathrm{Intact} - (k_m + k_p)\,\mathrm{DSB}_1, \qquad (6)$$

$$\frac{d\,\mathrm{Indel}}{dt} = k_m\,\mathrm{DSB}_1 + (k_m + k_p)\,\mathrm{DSB}_2 - k_{rc}\, Cas_t\,\mathrm{Indel}, \qquad (7)$$

$$\frac{d\,\mathrm{DSB}_2}{dt} = k_{rc}\, Cas_t\, \mathrm{Intact} - (k_m + k_p)\,\mathrm{DSB}_2, \qquad (8)$$

satisfying the normalization condition,

$$\mathrm{Intact} + \mathrm{DSB}_1 + \mathrm{DSB}_2 + \mathrm{Indel} = 1, \qquad (9)$$

and the initial condition:

$$\text{Intact}(0) = 1 - B_0,\ \text{DSB}_1(0) = B_0,\ \ \text{DSB}_2(0) = 0, \text{Indel}(0) = 0\,. \tag{10}$$

The experimentally measured DSB will be the sum of the two types of DSBs,

$$\text{DSB} = \text{DSB}_1 + \text{DSB}_2. \tag{11}$$

We solved both sets of equations (2-5) and (6-11). The theoretical DSB and indel curves were fitted to experimentally measured DSBs and indels vs *t* simultaneously with nonlinear least squares method in a single optimization problem that determined the model parameters for each locus as well as a single k_{deg}.

2. Analysis of 53BP1-mCherry arrival time at the single DSB site

Before uncaging, we assume that the fraction of DNA bound by Cas9/cgRNA is B_0 and the unbound fraction is $1 - B_0$. After uncaging, the Cas9-bound DNA results in DSB with a rate k_B, while the unbound fraction needs to be bound by Cas9/gRNA and then cut. Target search can be viewed as a chemical reaction with a rate k_s, which depends on the accessibility of the locus itself, and the concentration of Cas9/gRNA. Alternatively, the Cas9/gRNA binding events can be described stochastically as a Poisson process and the target search time t_s is an exponentially distributed random variable with mean value $\tau_s = 1/k_s$. After DNA is cut, the DSB will eventually be exposed, for example due to ejection of Cas9/gRNA, and DSB repair proteins will be deployed at the damage site. The first appearance of repair proteins, 53BP1 in our experiment, is viewed as the start of DNA repair. As a first order approximation, we assume that it is described by a single rate k_d. Therefore, the time from DNA being cut to the start of DNA repair is described by a random variable t_d, that is exponentially distributed with mean value $\tau_d = 1/k_d$. This is summarized in the following reaction scheme.

$$\underset{1-B_0}{\text{unbound DNA}} \xrightarrow{k_s} \underset{B_0}{\text{DNA} - \text{Cas9}} \xrightarrow{k_B} \text{DNA}^{\text{Break}} - \text{Cas9} \xrightarrow{k_d} \text{DNA}^{\text{Break}} - \text{Repair Protein} + \text{Cas9}$$

Experimentally, we measured the initial arrival time T_1 of a DSB repair protein, 53BP1, starting from *t*=0, the moment of cgRNA uncaging. From in vitro and in vivo experiments, we know that a pre-bound Cas9/gRNA cuts the DNA within seconds after activation, which is much faster than target search and DSB exposure and detection. Therefore, $k_B \gg k_s \text{ or } k_d$. So we ignore the time it takes for a pre-bound Cas9/gRNA to cut DNA. Taken this together, the first arrival time T_1 for repair proteins is defined as

$$T_1 = \begin{cases} t_d, & for\ bound\ fraction\ B_0 \\ t_{s+}t_d, & for\ unbound\ fraction\ (1 - B_0) \end{cases}. \tag{12}$$

Given t_s and t_d are exponentially distributed, the probability distribution function (pdf) of T_1 is given by

$$pdf(T_1) = \left(\frac{B_0}{\tau_d} + \frac{(1 - B_0)}{\tau_d - \tau_s}\right) \exp\left(-\frac{T_1}{\tau_d}\right) + \frac{(1 - B_0)}{\tau_s - \tau_d} exp\left(-\frac{T_1}{\tau_s}\right). \tag{13}$$

The distribution has three unknown parameters, B_0, τ_d and τ_s. We measured the fractional bound B_0 independently from fraction of DSB 1 minute after uncaging with ddPCR. We determine the parameters τ_d and τ_s by fitting the experimentally determined distribution of the first arrival time T_1 using maximum likelihood estimation. The expectation value of the first arrival time is

$$\langle T_1 \rangle = \tau_d + (1 - B_0)\tau_s. \tag{14}$$

After completion of the first round of repair, and if the repair is perfect or the resulting indel can be recut, we expect that active Cas9-gRNAs, generated by uncaging of gRNA, can search for the target site and cut it again. Because there is no pre-bound Cas9, the time gap T_{gap} between the end of a repair event and the beginning of the next repair is

$$T_{gap} = t_s + t_d, \tag{15}$$

which follows the distribution of

$$pdf(T_{gap}) = \frac{1}{\tau_d - \tau_s}\exp\left(-\frac{T_{gap}}{\tau_d}\right) + \frac{1}{\tau_s - \tau_d}exp\left(-\frac{T_{gap}}{\tau_s}\right). \tag{16}$$

Here, we have assumed that the search time follows the same distribution as the first round of search. The expectation value of T_{gap} is simply $\langle T_{gap}\rangle = \tau_s + \tau_d$. We can relate the mean values of T_1 and T_{gap} by

$$\langle T_{gap}\rangle = \langle T_1\rangle + B_0\tau_s. \tag{17}$$

So, we expect that the mean value of the gap time (T_{gap}) should be longer than the first arrival time for $B_0\tau_s$ which is confirmed by the experimental data (Table S8).

Supplementary figures and captions

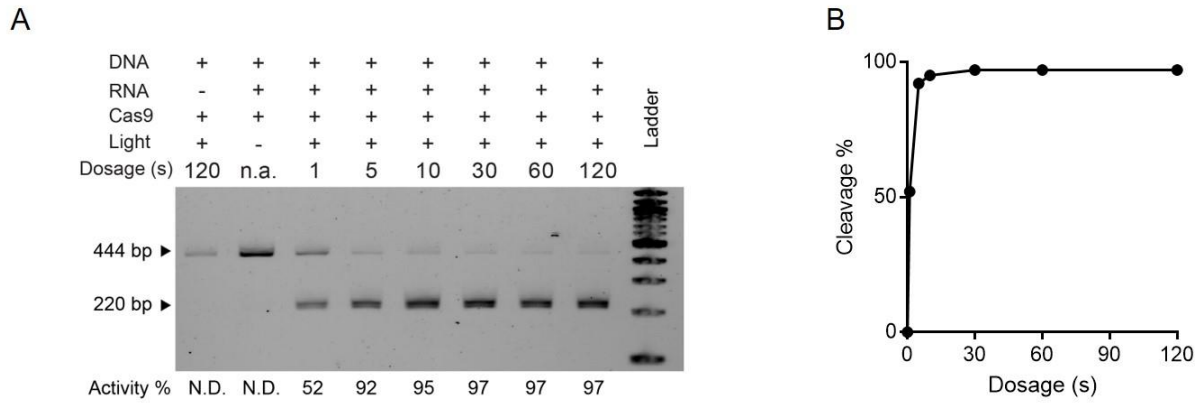


Fig. S1. Light-inducible cleavage activity of Cas9/cgRNA is dosage dependent. (A) *In vitro* cleavage assay showing dosage-dependent DNA cleavage activity. Samples were incubated at 37 °C for 30 min after light stimulation of indicated duration (dosage). (B) Quantification of Cas9 cleavage activity from panel A as cleavage percentage, performed using the ImageJ gel analysis program.

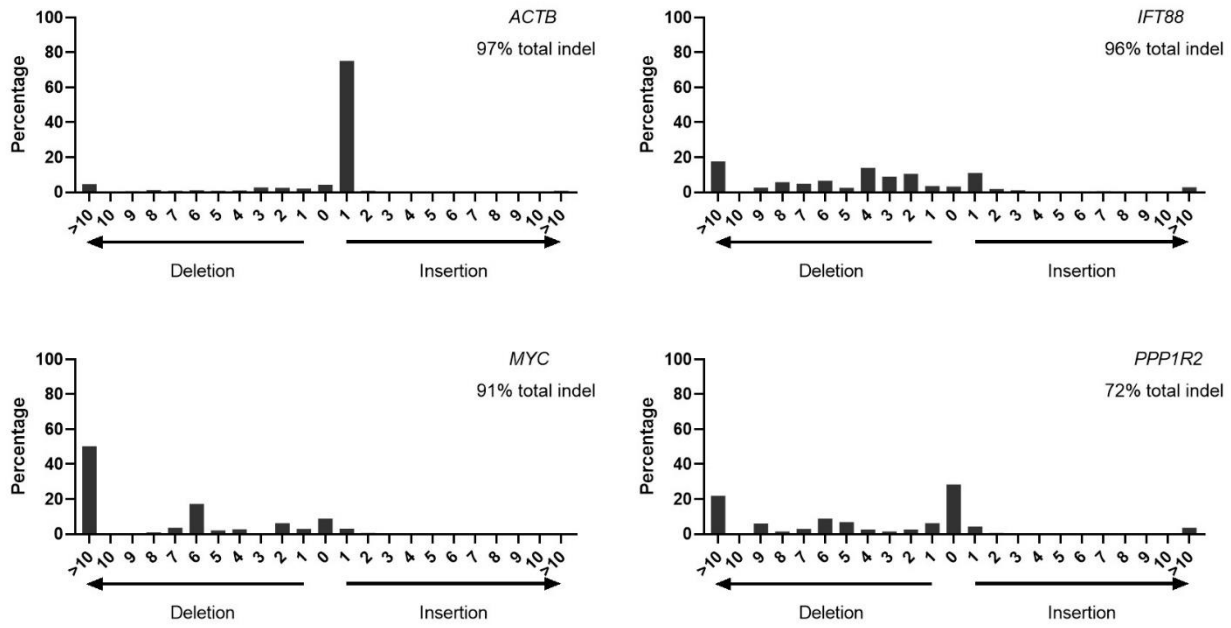


Fig. S2. Insertion and deletion profiles at 4 different loci. The *ACTB* cleavage site predominantly contained +A insertions, while all others cleavage sites (*IFT88*, *MYC*, *PPP1R2*) mainly accrued larger deletions. The bars represent averaged data across the triplicate data points found in Figure 1E. 6,421 to 23,524 paired-end amplicon sequencing reads were obtained per sample.

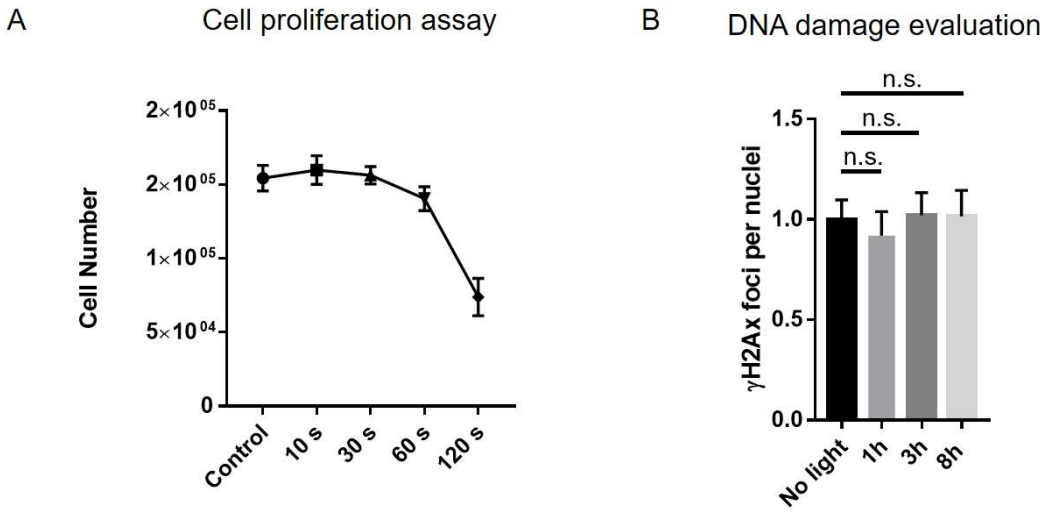


Fig. S3. Measurement of phototoxicity induced by 365 nm light. Cell proliferation assays were performed on HEK293T and U-2 OS cells after stimulation with 365 nm light of different dosages (seconds of exposure at equal light power). (A) HEK293T cells were harvested two days later and flow cytometry was used to count the cells (n=3 biological triplicates). (B) Immunofluorescence microscopy was performed to assess the number of phosphorylated H2AX foci in U-2 OS without light stimulation and after 30 s 365 nm light stimulation. Cells were fixed at 1, 3 and 8 h after stimulation for the assay (n>100 cells for 5 technical replicates, foci number normalized to no light control). Error bars represent standard error of the mean in both plots.

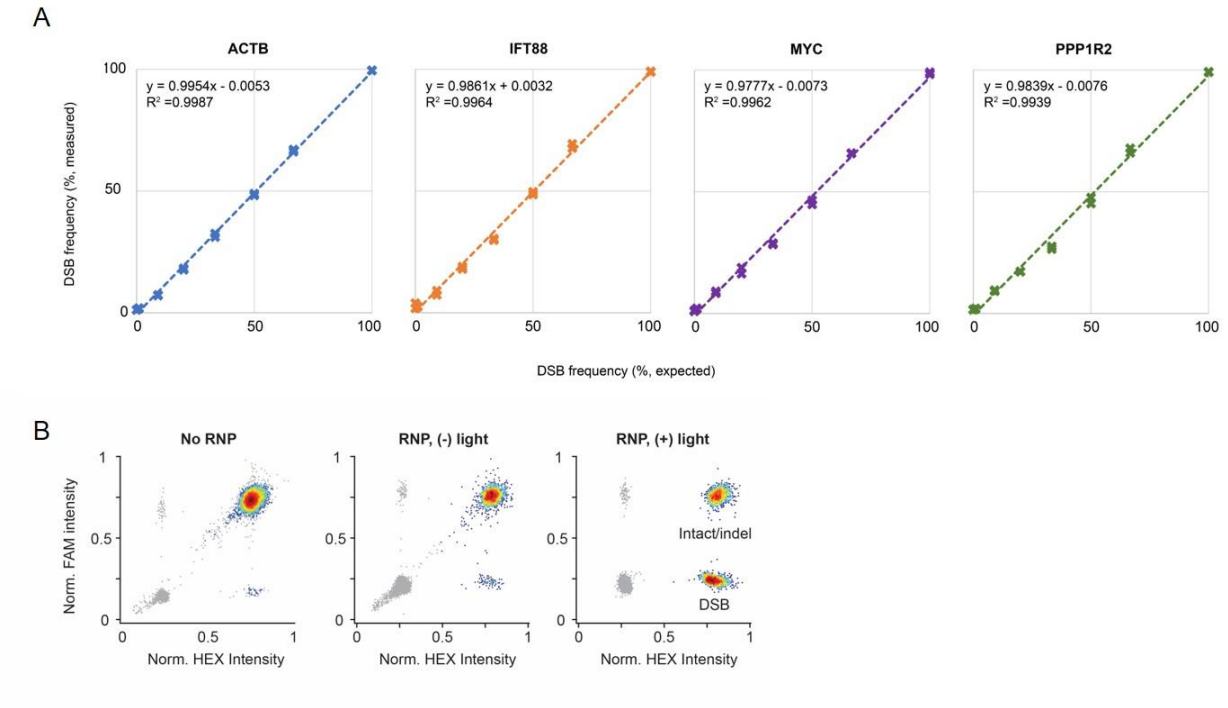


Fig. S4. DSB-ddPCR accurately reports the percentage of DNA cleavage. (A) Standard curves demonstrate the linear relationship between the expected DSB frequency and the DSB frequency measured by the DSB-ddPCR assay at *ACTB*, *IFT88*, *MYC*, *PPP1R2*. Regression was computed using data from technical duplicates. (B) Representative droplet FAM and HEX probe intensities for cells without electroporation of RNPs (left panel), with RNP but no light stimulation (middle panel), and with RNPs and 30 sec post light stimulation (right panel). Grey points indicate droplets with either no DNA templates or no probes (bottom left), or with just reference probe (FAM) (top left), and are not considered in the analysis. Colored points indicate droplets with intact/indel genomic DNA with both FAM and HEX probes (top right), or droplets with DSB-containing genomic DNA and/or with only HEK probe (bottom right). Color gradient from blue to red corresponds to increasing point density.

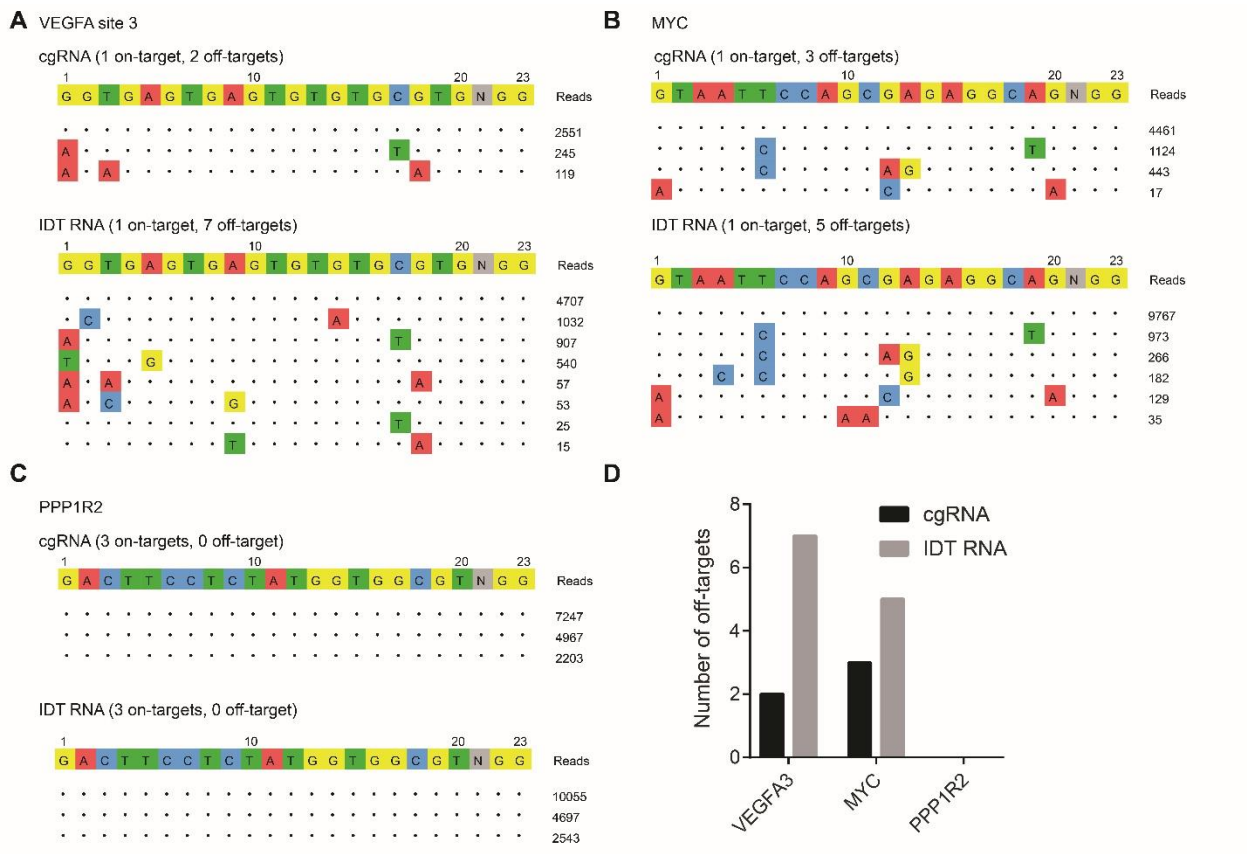


Fig. S5. Off-target analysis using GUIDE-seq at 3 different loci. (A-C) Figure displaying both on- and off-target sites for cgRNA and wild type control (cr/trRNA purchased from IDT) for three target sequences in *VEGFA*, *MYC*, and *PPP1R2*. The number of raw reads was normalized between cgRNA and wild type control. (D) Summary graph comparing the number of off-target sites between cgRNA and wild type control at each target sequence. Sequencing data for all samples are available under BioProject Accession PRJNA609749. Table S10 contains the raw off-target results used to generate the plots in panels A-C.

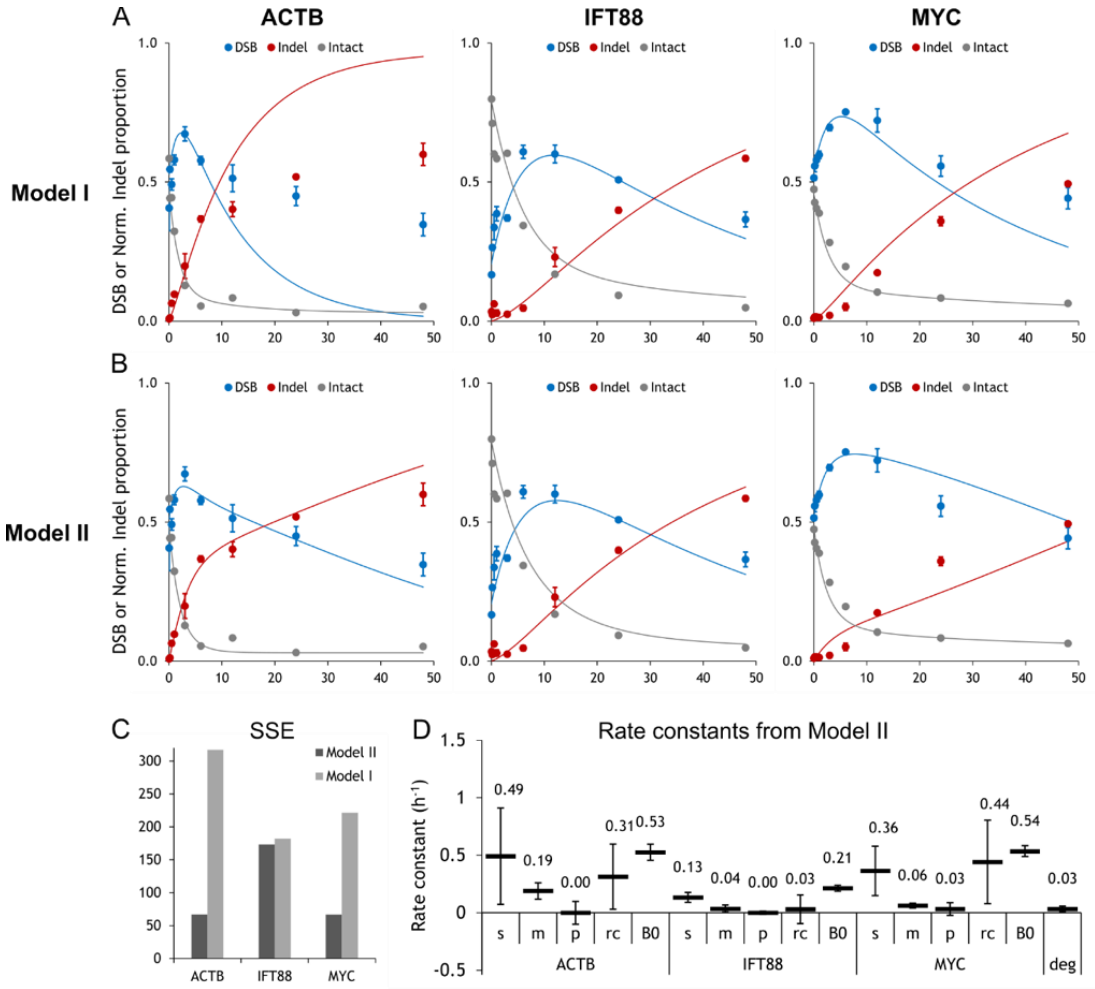


Fig. S6. Kinetic modeling of Cas9-induced DSB and indel formation. Full description of kinetic modeling is found in Supplementary Theory. Cas9/cgRNA RNPs targeting 3 different loci were electroporated into HEK293T cells respectively. Light stimulation occurred 12 h after electroporation, and genomic DNA was harvested at multiple time points after light stimulation. ddPCR and TIDE analysis were used to quantify the percentage of DSB and indels as a function of time. (A-B) The round data points correspond to DSB (blue) and indel (red) measurements as a function of time after light activation at time 0, for 3 target sequences (*ACTB*, *IFT88*, *MYC*). The intact fraction (grey) was inferred from DSB and indel measurements. Error bars represent standard error of the mean (n=3 biological replicates). The solid lines correspond to model fitting with either Model I (A) or Model II (B). Model II factored in re-cleavage of indel (k_{rc}) whereas Model I did not. Normalized indel percent is defined as the percent of total DNA at each locus with indels (factoring in cleaved DNA that cannot be amplified for indel detection). Norm. Indel % = Indel % × (100 – DSB %)/100. Intact % = 100 - Indel % - DSB % (the sums of DSB %, Normalized Indel % and Intact % equals 100 %) (C) Plot of sum of squared errors of prediction (SSE) for Models I and II. Lower values indicate better fitting. (D) Plot of model parameters determined from fitting. 's' indicates k_s, 'm' indicates k_m, etc.; 'B0' is the initial cleavage percent determined experimentally; 'deg' indicates k_{deg}. Error bars indicate 95% confidence intervals.

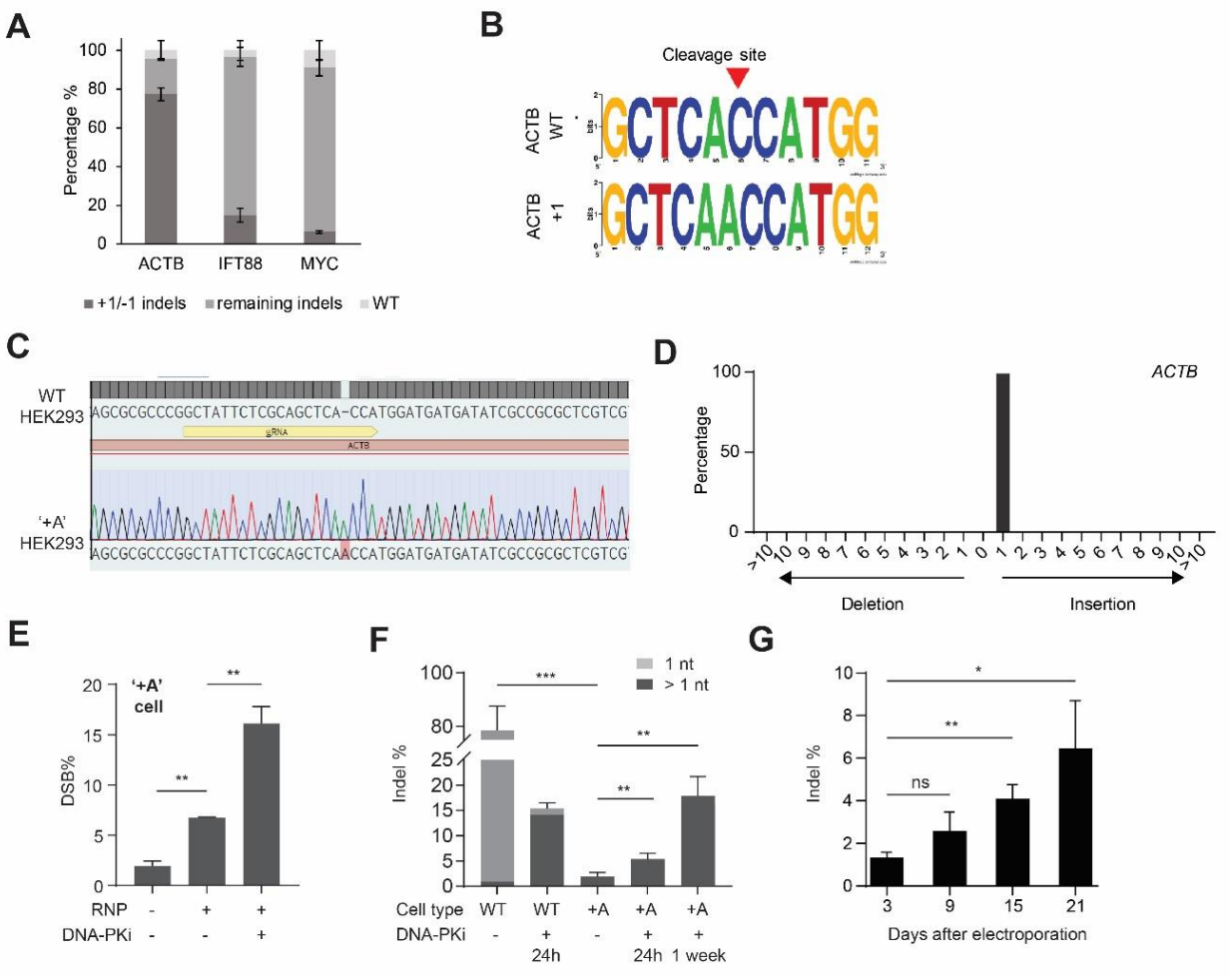


Fig. S7. Characterization of the monoclonal HEK293T cell line with a single +1 adenosine insertion at the ACTB locus. (A) Targeted deep sequencing revealed that a significant percentage of indels are +1 insertion or –1 deletion at three loci 48 h after Cas9 activation. WT represents the percentage of DNA with no mutation. (B) At the *ACTB* locus, 97.3 ± 1.3 % of +/–1 indels are +1 'A' insertions (https://weblogo.berkeley.edu/logo.cgi). (C) We expanded a monoclonal cell line harboring +A insertions at the ACTB cleavage site from a previous round of Cas9 editing. Genomic DNA from the +A monoclonal HEK293T cell line was extracted and Sanger sequenced. (D) TIDE analysis from Sanger sequencing yielded a pure, single adenosine insertion. (E-G) We performed additional rounds of Cas9 editing to this +A cell line using Cas9/cgRNA. DNA-PKi denotes inhibition of DNA-PKcs with KU-0060648. DNA-PKcs requires autophosphorylation for NHEJ to proceed with ligation and complete repair – DNA-PKcs inhibitors have been shown in past literature to inhibit autophosphorylation, leading to stalling of efficient repair and persistence of unrepaired DSBs (*31-34*). Brinkman et al, *Mol Cell*, 2018 further showed that DNA-PKcs inhibition led to re-direction of repair from classical NHEJ to MMEJ, which they suggest to have a slower repair rate (*17*). Our hypothesis is that after +A cleavage, the DSB is repaired via the classical NHEJ pathway. DNA-PKcs inhibition will stall completion of c-NHEJ repair, leading to higher DSBs at earlier time points, while also diverging repair through MMEJ, leading to higher indels at end point due to a more mutagenic pathway. (E) DSBs in +A cells at 6 h after 1 additional round of Cas9/cgRNA delivery. DNA-PKcs inhibition increased the DSB %, consistent with

stalling of efficient repair. (F) Indels at 24 h after 1 additional round of Cas9/cgRNA delivery in +A and wild type (non +A) cells. Indel species are distinguished between 1 nt or >1 nt. DNA-PKcs inhibition increased the indel %, consistent with eventual repair through the more mutagenic MMEJ pathway. (G) Despite very low indel generation in +A cells without drug and one round of Cas9/cgRNA delivery, Cas9/cgRNA delivery every 3 days over a course of 21 days led to an increase in indels in +A cells. Error bars in panels A, E, F and G represent standard deviations (n=3 biological replicates).

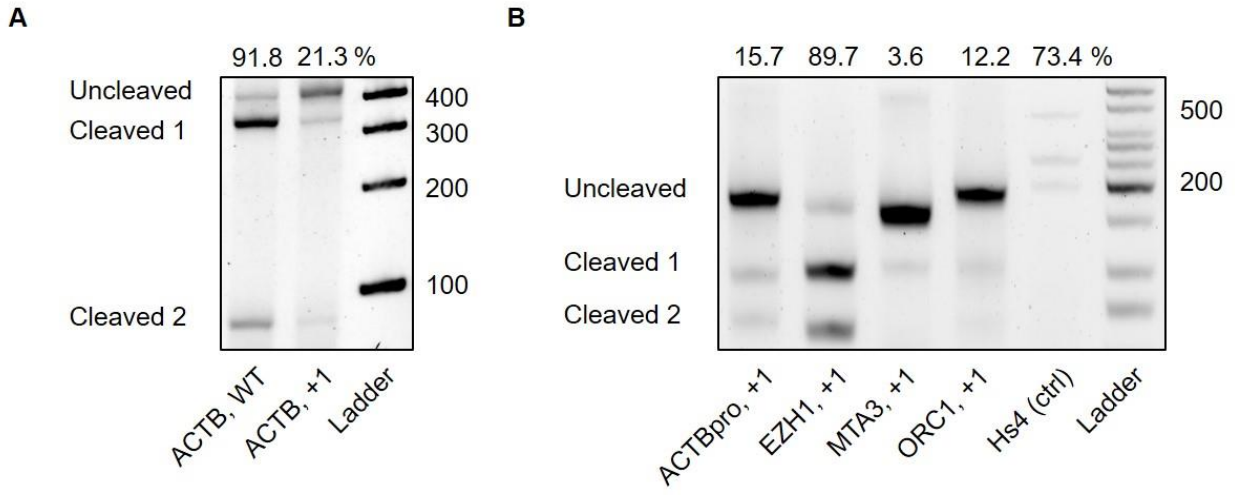


Fig. S8. In vitro cleavage assay showing Cas9 cleavage of +1 indel products. (A) Cleavage of WT and +1 *ACTB* target sequences in a representative gel. '*ACTB*, +1' indicates one A insertion at the cut site (4th position from PAM). (B) Four additional loci that form +1 insertion at the cut site (*35*) demonstrated different levels of cleavage efficiencies from 3 % to 90 %. '*ACTBpro*, +1' and 'EZH1, +1' have an A insertion at their cut sites. '*MTA3, +1*' and 'ORC1, +1' have a T insertion at their cut sites. All DNA substrates used were purchased from GenScript as dsDNA fragments. Each sequence fragment was taken from the human genome and includes the respective cut site (Table S2).

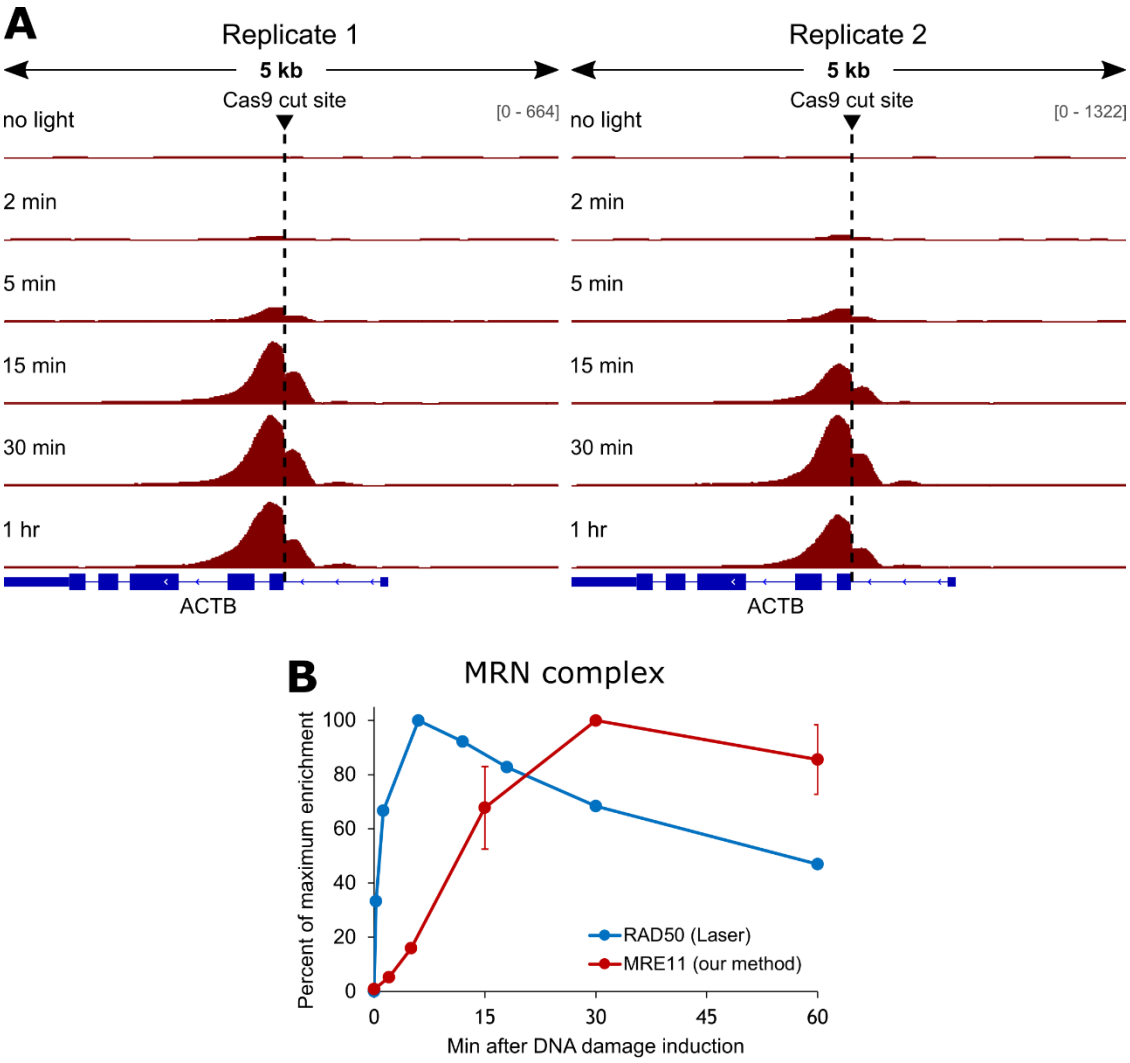


Fig. S9. Additional genome browser snapshots of MRE11 ChIP-seq and its benchmarking to published laser microirradiation data. (A) Snapshot of MRE11 enrichment in a 5 kb window centered on the *ACTB* cleavage site as a function of time after Cas9 activation. Results for both ChIP-seq replicates are shown. (B) Fragments per million in the 5 kb region around the *ACTB* cleavage site over time (panel A of this figure; summary statistics in Fig. 2C) was compared to RAD50 average foci intensity after laser microirradiation to HeLa Kyoto cells (from Aleksandrov et al, *Mol Cell*, 2018 – data downloaded from http://dnarepair.bas.bg/index.php/all-protein/ with the "no bleach" option). Error bars represent standard error of the mean (n=2 biological replicates). Because different readouts were employed for each method, each measurement was normalized by its maximum to yield percent of maximum enrichment for appropriate comparison. MRE11 and RAD50 are believed to be recruited to DSBs together as part of the MRN (Mre11-Rad50-Nbs1) complex.

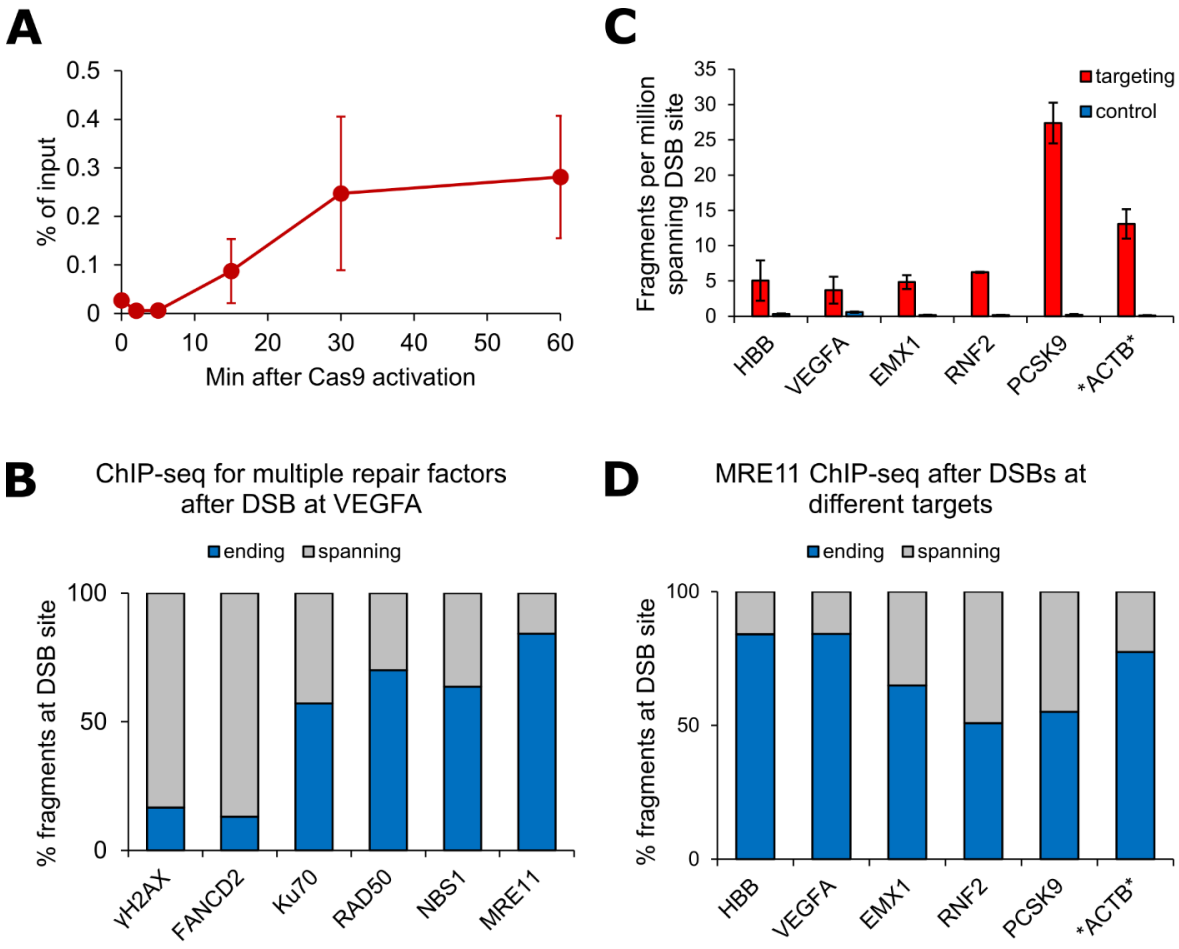


Fig. S10. Further validation that MRE11 remains bound to DNA after ligation. (A) Probe-based qPCR detected enrichment of MRE11 ChIP DNA that spans the *ACTB* cleavage site starting from 15 min after Cas9 activation. (B) Using publicly available datasets (BioProject Accession PRJNA509652) generated for the DISCOVER-seq manuscript (*18*), specifically ChIP-seq for multiple DSB repair factors after Cas9 targeting *VEGFA*, the percent of fragments either spanning the cleavage site (grey), or starting or ending within a 10 bp window around the cut site (blue), was calculated for each DNA repair factor. Our analysis of PRJNA509652 recapitulated their published results (Fig. S3A of their manuscript), which helped confirm the correctness of our analysis software. (C) Fragments per million spanning the DSB site from MRE11 ChIP-seq (PRJNA509652) with Cas9 targeting 5 different loci in 2 different cell types (K562 for *HBB*, *VEGFA*, *EMX1*, *RNF2* and mouse liver for *PCSK9*) compared to MRE11 ChIP-seq generated for this manuscript (PRJNA609749) of HEK293T cells 60 min after light-activation of Cas9/cgRNA targeting *ACTB* (**ACTB**). The population of DNA fragments that span each DSB site (red) was significantly higher than background (green; BFP non-targeting control for PRJNA509652, no-light control for PRJNA609749). Inclusion of non-targeting controls was essential to verify that the spanning fragments cannot be attributed to merely ChIP-seq background. (D) The analysis in panel B was performed on the data in panel C. The percent of spanning fragments ranged from ~15 % to ~50 %. Results at *ACTB* generated for this manuscript was consistent with the 5 other DSB sites in published literature (*18*). Error bars in panels A and C represent standard error of the mean (n=2 biological replicates).

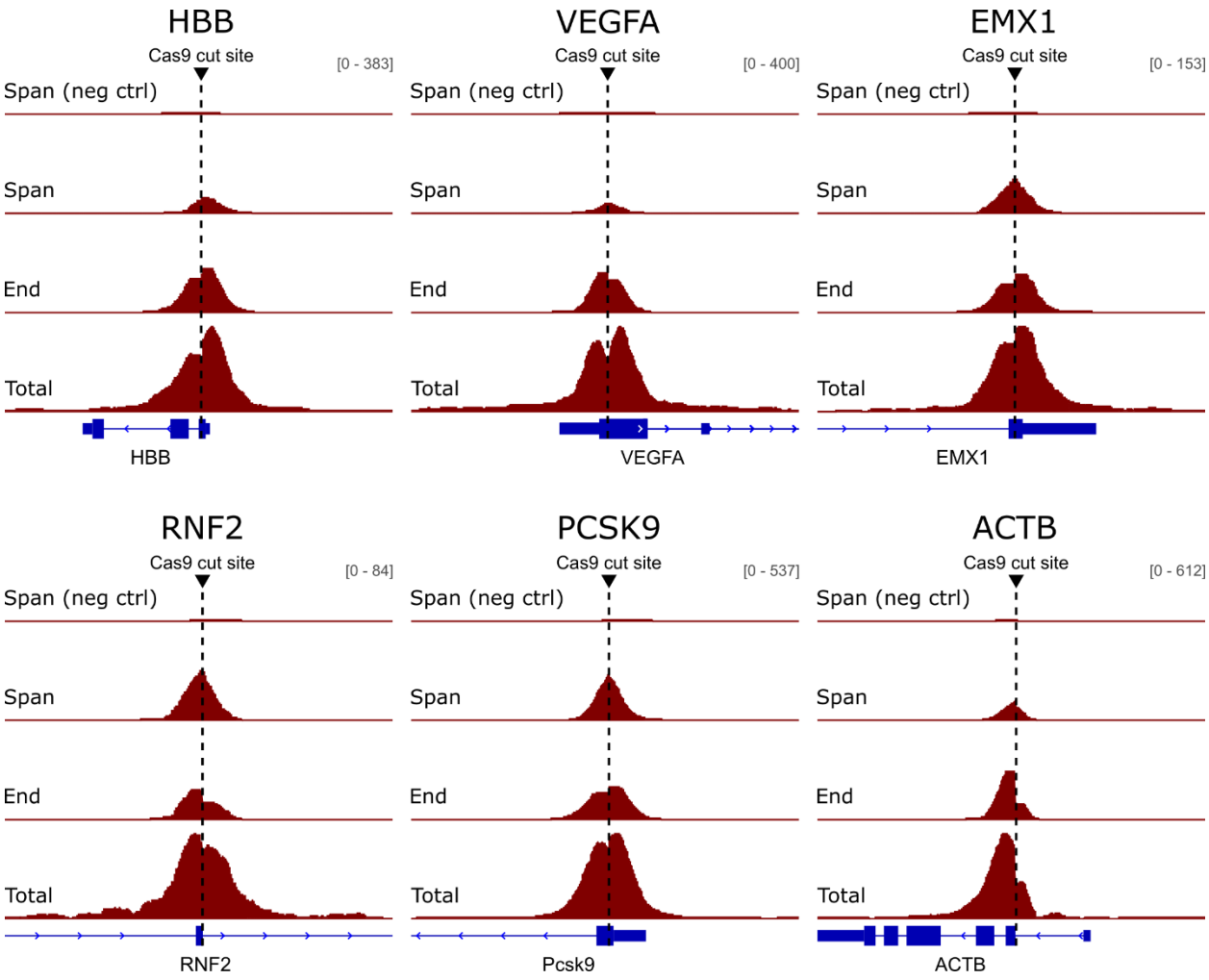


Figure S11. Genome browser snapshots of reads that span cut site, end at cut site, and total reads for 6 Cas9-induced DSB sites. For *HBB*, *VEGFA*, *EMX1*, *RNF2*, and *PCSK9*, MRE11 ChIP-seq after Cas9 cleavage of each target, along with a BFP nontargeting negative control, were used (PRJNA509652) (*18*). For *ACTB*, MRE11 ChIP-seq 1 hour after light activation of Cas9/cgRNA targeting *ACTB*, along with a no-light negative control, was used (PRJNA609749). For each target sequence, fragment pileups were generated in a 5 kb window centered at each cut site from paired-end reads that either spanned the cut site ("Span"), began or ended in a 10 bp window centered on the cut site ("End"), or all reads in the 5 kb window ("Total"). Fragment pileups of spanning reads from the appropriate negative control sample were included for comparison ("Span (neg ctrl)"). Spanning fragments consistently represent a significant fraction of total MRE11 reads and cannot be attributed to ChIP-seq background. These results suggest that the population of MRE11-bound DNA that spans the DSB site after Cas9 cleavage generalizes to other target sequences and cell types.

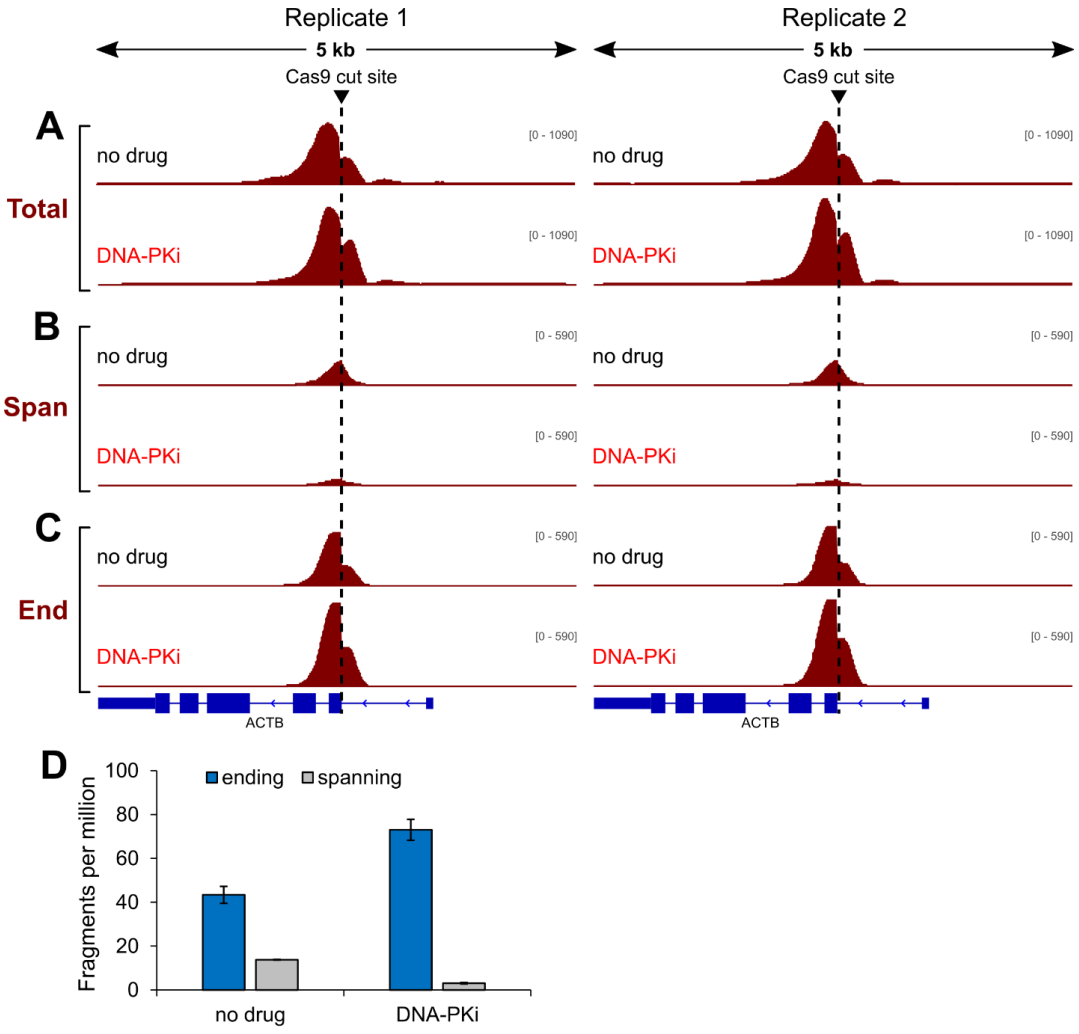


Fig. S12. DNA-PKcs inhibition greatly reduced spanning fragments and increased fragments that begin or end at DSB site. DNA-PKcs requires autophosphorylation for NHEJ to proceed with ligation and complete repair – DNA-PKcs inhibitors are known to inhibit autophosphorylation, leading to stalling of efficient repair and persistence of unrepaired DSBs (*31-34*). Our hypothesis is that MRE11 persists on genomic DNA that was recently repaired through a DNA-PKcs dependent pathway, as represented by a population of MRE11-bound DNA that spans the DSB site. We predict that DNA-PKcs inhibition will stall repair, leading to depletion of this "spanning population" and increase in the "unrepaired population", or fragments derived from unrepaired DSBs (*18*). (A) MRE11 ChIP-seq fragment pileups in a 5 kb window centered at the *ACTB* DSB site 2 hours after activation of Cas9/cgRNA targeting *ACTB* in HEK293T cells. DNA-PKi denotes inhibition of DNA-PKcs with KU-0060648. (B) Fragment pileups of the "spanning population", which we attribute to recently-repaired MRE11-bound genomic DNA. (C) Fragment pileups of the "unrepaired population", defined to be those that start or end within a 10 bp window centered at the DSB site, which attributed to MRE11-bound, un-repaired DSBs (*18*). (D) Quantification of panels B and C in fragments per million. DNA-PKcs inhibition depleted the "spanning population" (grey) and increased the "unrepaired population" (blue), which is consistent with our hypothesis. Error bars represent standard error of the mean (n=2 biological replicates).

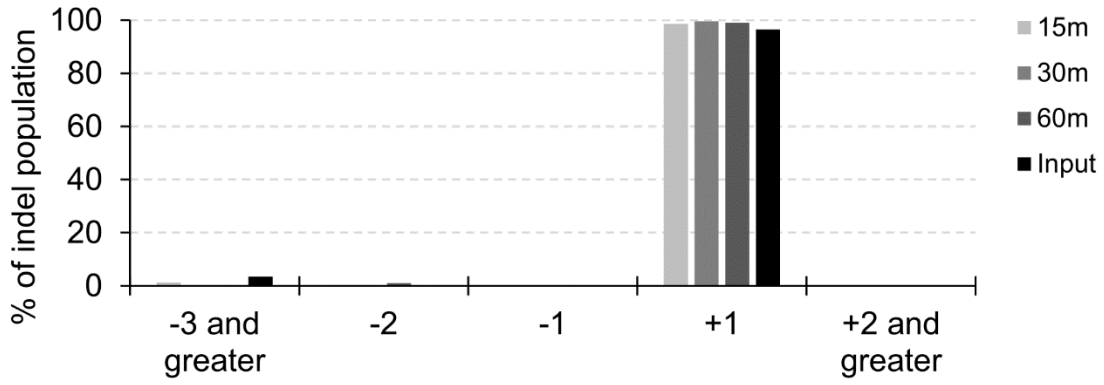


Fig. S13. Percent of each indel species out of the total indel population from deep sequencing of PCR products that amplify through the cut site. Evaluation of both ChIP input at 60 min ("Input") and MRE11 ChIP DNA at 15 min, 30 min, and 60 min after activation of Cas9/cgRNA targeting *ACTB* revealed comparable distribution of +1 insertion indels, suggesting that ligated, MRE11-bound DNA is the major repair pathway product that leads to the observed indel distribution.

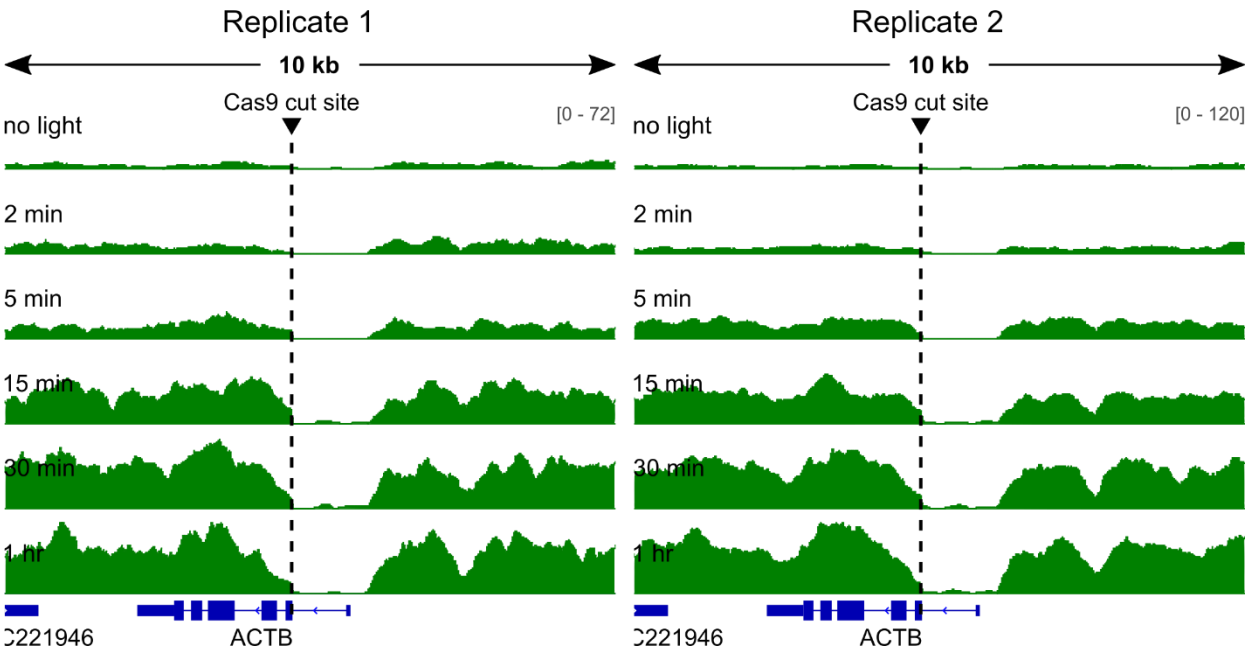


Fig. S14. Additional genome browser snapshots of γH2AX ChIP-seq. Snapshot of γH2AX enrichment in a 10 kb window centered on the ACTB cleavage site as a function of time after Cas9 activation. Results for both ChIP-seq replicates are shown. Depletion of γH2AX immediately flanking the cleavage site is consistent with previous literature (*36-38*).

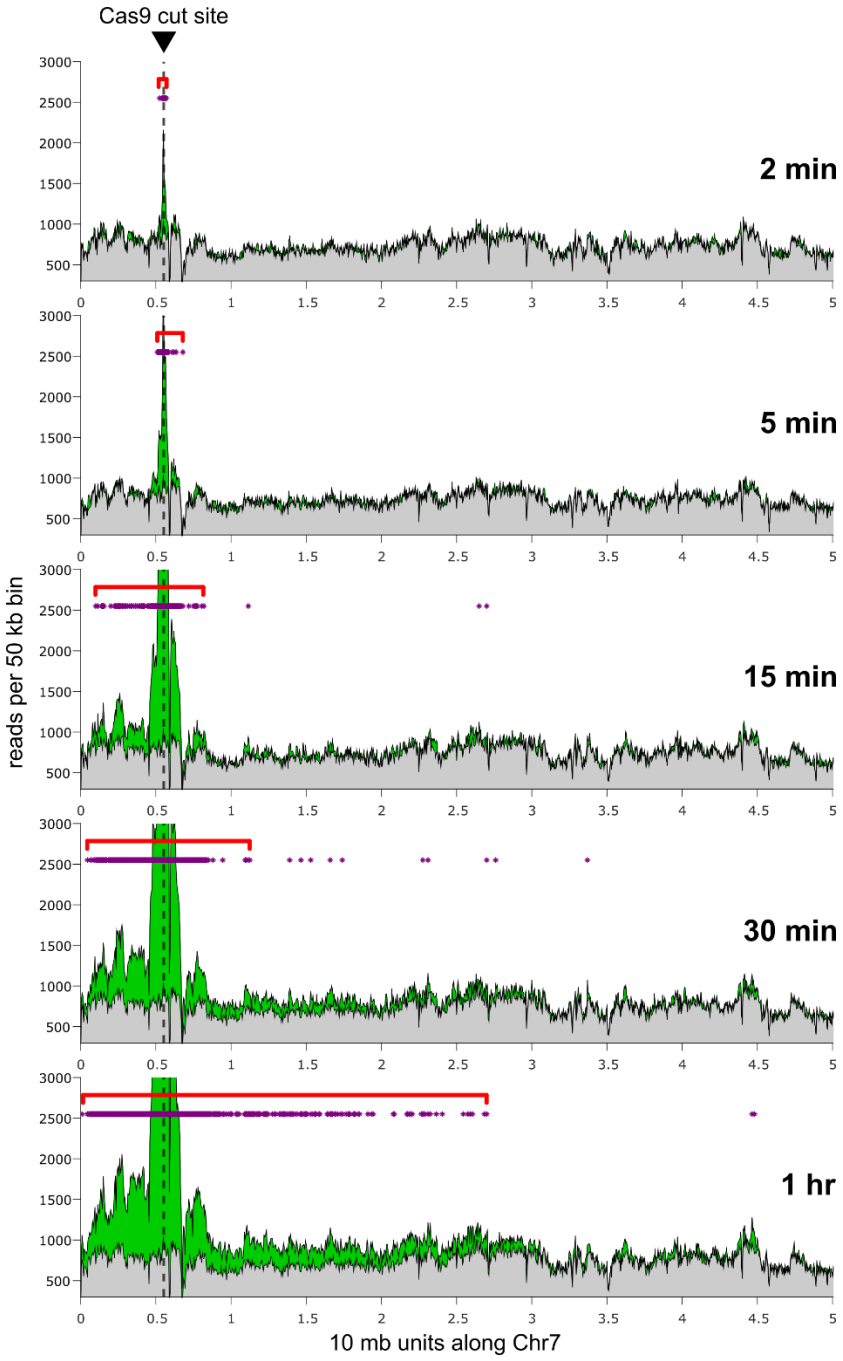


Fig. S15. Binning analysis of γH2AX ChIP-seq. Reads were binned at 50 kb, and each post-Cas9 activation time point was plotted (green) with no-light control overlaid (grey). For each bin, Student's *t*-test was performed ($p < 0.05$, paired, one-sided, Bonferroni correction, all post-Cas9 activation samples versus no-light control) using 1 kb sub-bins (fifty total). Significantly different reads in each bin between Cas9-activated versus no-light are labeled with purple asterisks. The entire enrichment width (red bar) is defined by the set of significantly different bins that spans from cleavage site to where the closest distance between two significant bins is < 2 mb.

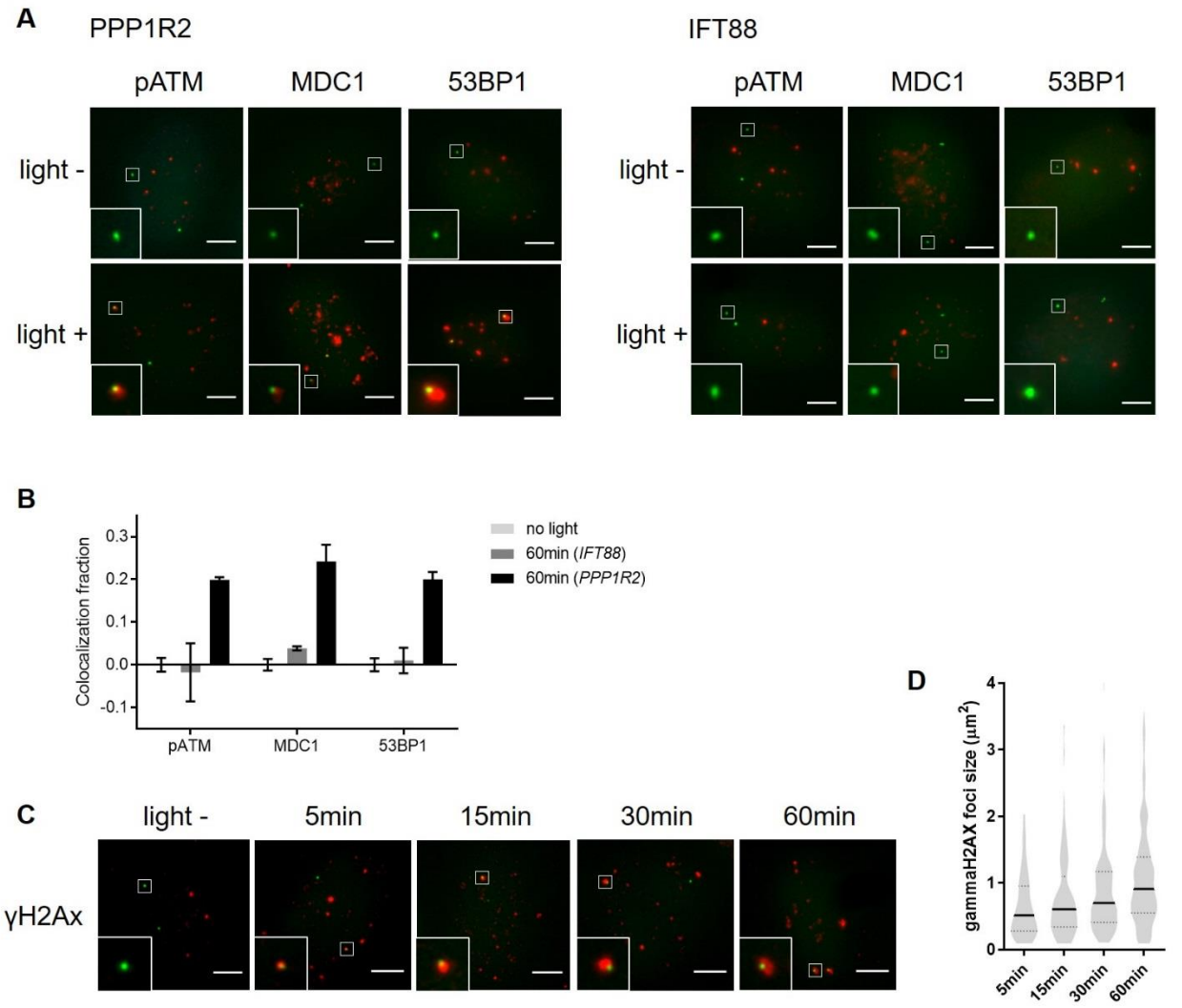


Fig. S16. Multiple DNA damage response proteins are recruited to a single Cas9 cleavage site after activation. U-2 OS monoclonal cells co-expressing Cas9-EGFP and 53BP1-mCherry were co-transfected with 11-mer sgRNA to label Ch3Rep and 20-mer cgRNA for light activation of a single DSB at either *PPP1R2* or *IFT88*. (A) Fluorescence microscopy was used to visualize the colocalization between Cas9-EGFP labeled Ch3Rep (green, EGFP) and several endogenous foci-forming DDR proteins including phosphorylated ATM, MDC1, and 53BP1 via immunofluorescence (red, Cy5). cgRNA targeting *IFT88* gene (located in Chr13) was used as negative control. Only light stimulation to cgRNA targeting *PPP1R2*, but not *IFT88*, exhibited colocalization with Ch3Rep, suggesting that colocalization is due to direct binding of repair proteins to a specific DSB site, and not due to IF background or light stimulation itself. (B) The fractions of Cas9 foci colocalized with pATM, MDC1 or 53BP1 were measured without light and 60 min after light stimulation (n > 150 alleles from three replicates). Error bars represent standard error of the mean (n > 150 alleles from 3 biological replicates). (C) Representative immunofluorescence images highlighting the change in phosphorylated H2AX foci size at the *PPP1R2* site, (D) quantified at different time points: solid lines: median foci size at each timepoint (n > 400 foci from 10 field-of-views from different sample slides). Scale bars, 5 μm.

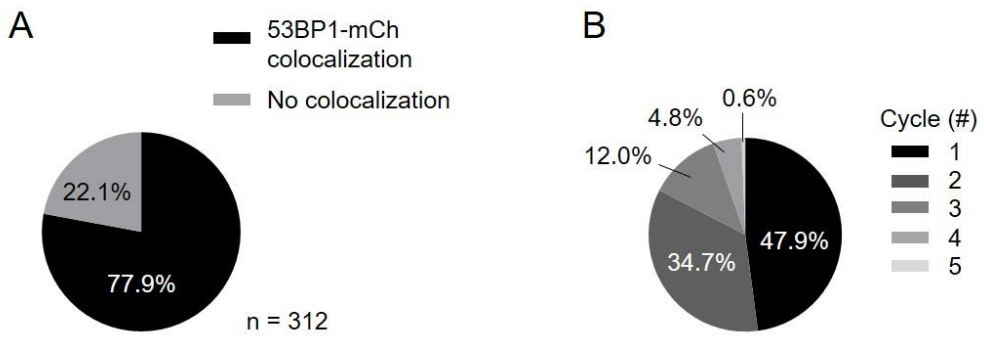


Fig. S17. 53BP1-mCherry foci colocalize with the DSB site at *PPP1R2*, often over multiple cycles. (A) Majority of *PPP1R2* alleles exhibit 53BP1-mCherry foci formation at some point for the duration of 8 hours after Cas9-EGFP/cgRNA activation, as measured by colocalization with the nearby Ch3Rep (n = 312 alleles, 5 biological replicates). (B) Number of 53BP1-mCherry foci cycles at each *PPP1R2* allele over the course of 8 hours after Cas9-EGFP/cgRNA activation (n =167 alleles, 5 biological replicates). The majority of alleles exhibit more than one 53BP1 cycle.

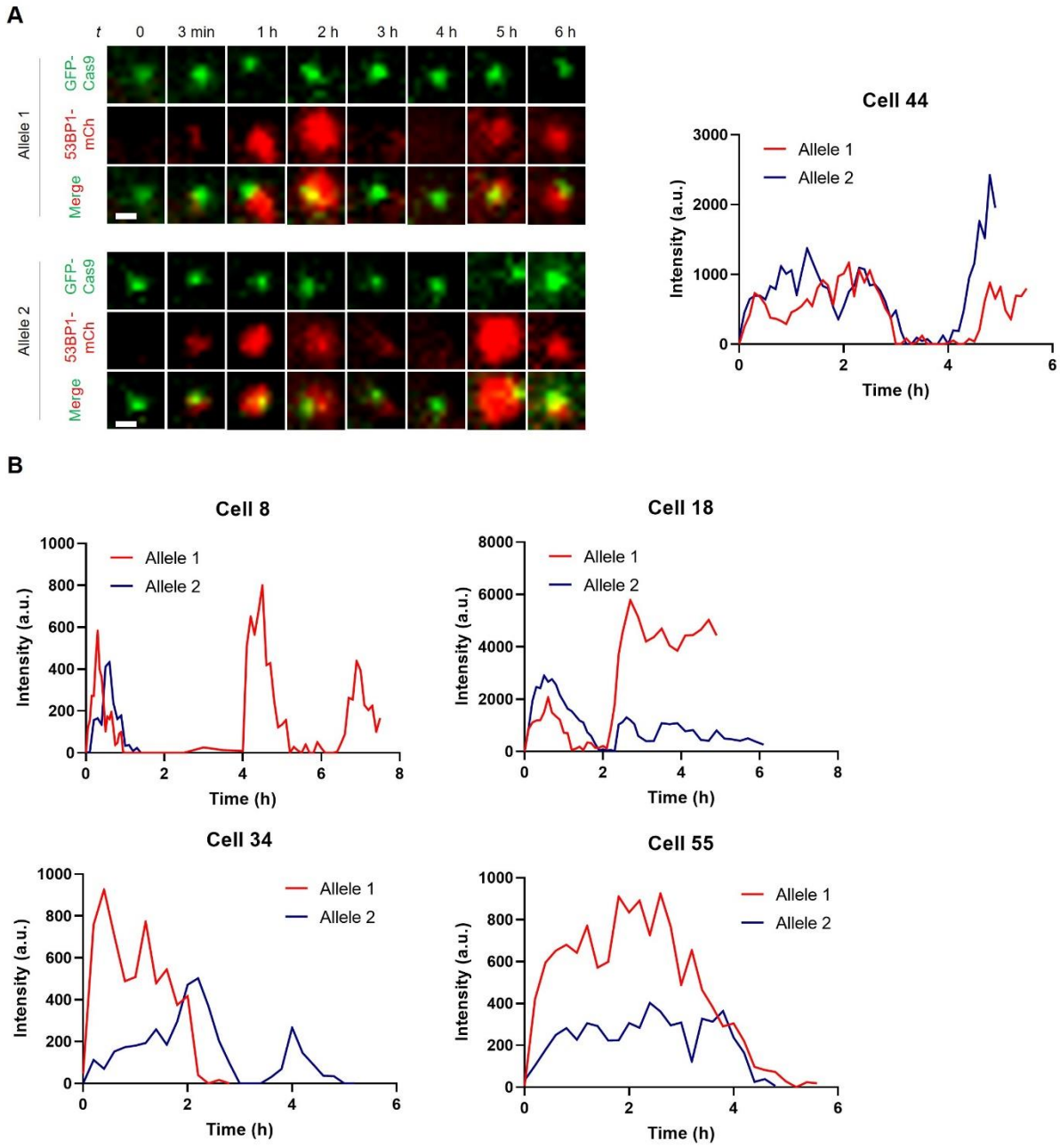


Fig. S18. The dwell time of 53BP1 foci was correlated between two alleles in the same nucleus. The cell numbers listed here correspond to those from Figure 3F. (A) Representative images and fluorescence intensity traces of 53BP1-mCherry at two alleles in cell #44, revealing correlated dwell times. Scale bar, 0.5 μm. (B) Raw intensity traces of 53BP1-mCherry from cell #8, #18, #34 and # 55, show more examples of correlated 53BP1 dwell times between alleles of the same cell.

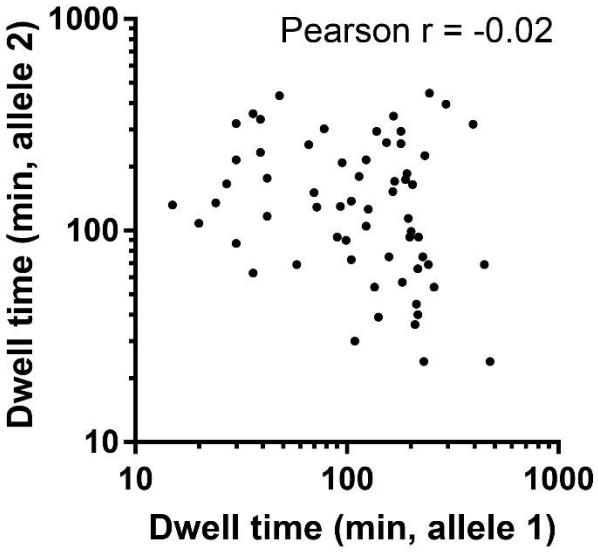


Fig. S19. Pearson correlation anaylsis showing no correlation of dwell time between two random alleles (r = -0.02).

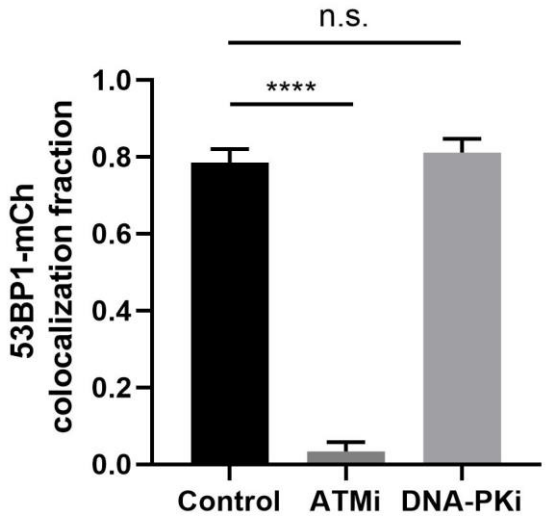


Fig. S20. The effect of inhibiting ATM or DNA-PKcs on 53BP1-mCherry recruitment at *PPP1R2*. ATM was inhibited using 100 μM KU-0055933 for 1 h before light stimulation (ATMi; n = 86 alleles, 2 biological replicates). DNA-PKcs was inhibited using 10 μM KU-0060648 before light stimulation (DNA-PKi; n = 134 alleles, 3 biological replicates). Control samples were subject to light stimulation without any treatment (n = 312 alleles, 5 biological replicates). Error bars represent standard deviation.

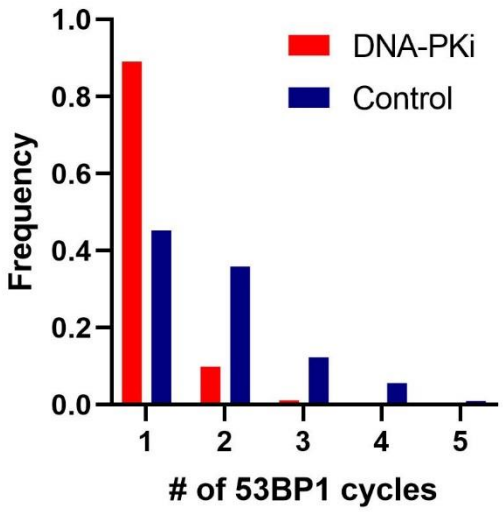


Fig. S21. Number of 53BP1-mCherry foci cycles appearing at single *PPP1R2* alleles, with or without 10 μM of DNA-PKcs inhibitor KU-0060648. Number of 53BP1-mCherry foci cycles after activation of Cas9-EGFP/cgRNA targeting *PPP1R2*, with or without DNA-PKcs inhibitor (DNA-PKi). n = 167 foci, 5 biological replicates for control; n = 92 foci, 3 biological replicates for DNA-PKcs inhibition.

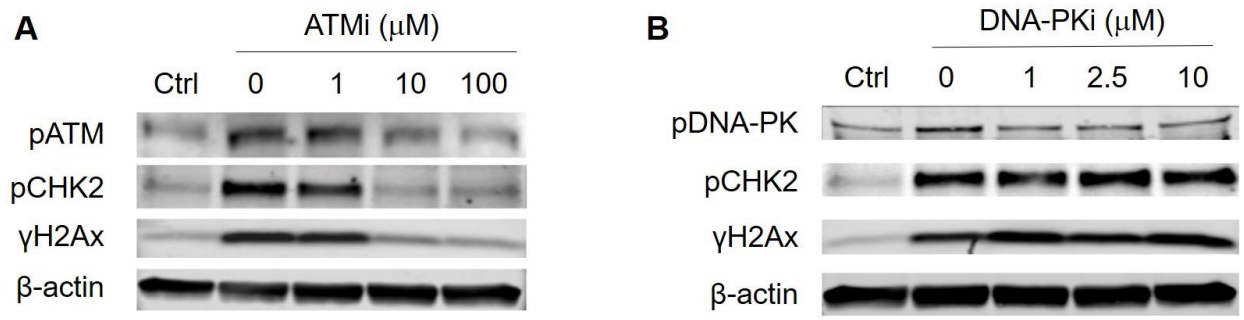


Fig. S22. Western blotting showing that ATM and DNA-PKcs inhibitors effectively block the activities of ATM, DNA-PKcs kinases and their downstream proteins, respectively. U-2 OS cells were treated with DMSO, ATM inhibitor KU-0055933 (ATMi) and DNA-PKcs inhibitor KU-0060648 (DNA-PKi) for 1 h before subject to 5 Gy of X-ray irradiation. After 30 min, proteins were collected from cell lysate and compared to those from negative control cells not treated with drugs and irradiation. (A) The phosphorylation level of ATM (Ser1981), CHK2 and H2AX were significantly reduced at concentrations of KU-0055933 higher than 10 μM. (B) KU-0060648 inhibits the phosphorylation DNA-PKcs (Ser2056) at concentrations higher than 1 μM without affecting that of CHK2 activation and gamma H2AX.

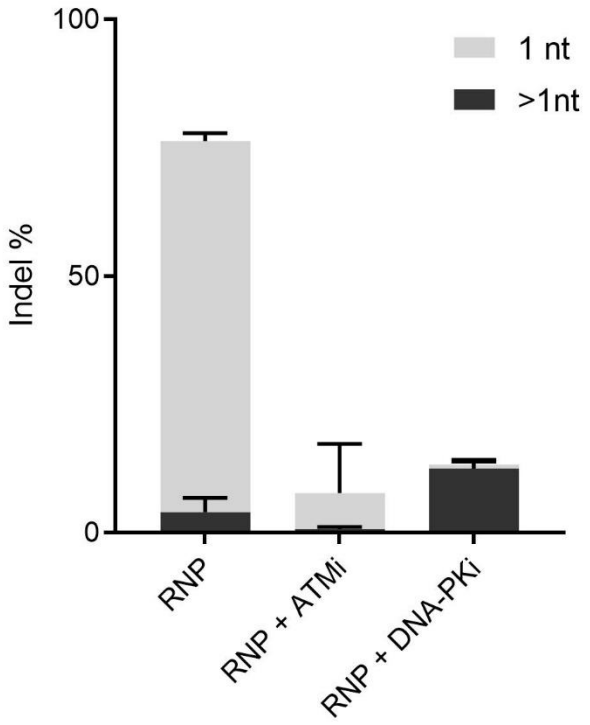


Fig. S23. Effects of ATM and DNA-PKcs inhibition on repair outcomes at the *ACTB* cleavage site. ATM was inhibited using 100 μM KU-0055933 (ATMi). DNA-PKcs was inhibited using 10 μM KU-0060648 (DNA-PKi). Error bars represent standard deviation (n=2 biological replicates).

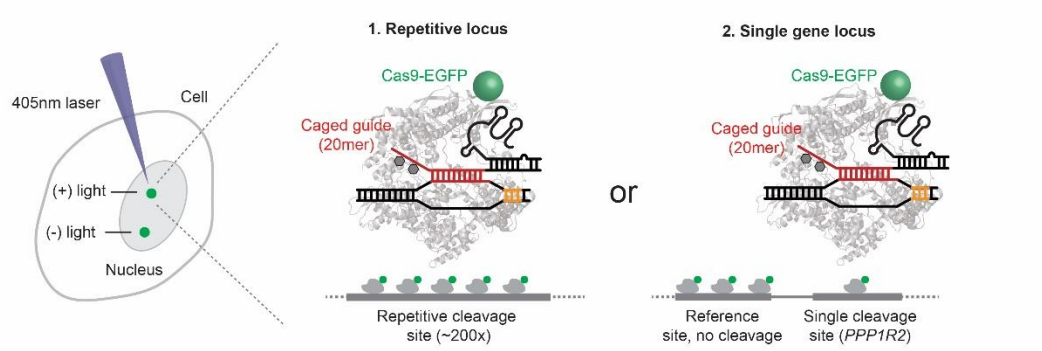


Figure S24. Schematic showing imaging-guided DSB induction at a specific genomic sequence on a single allele. A monoclonal U-2 OS cell line co-expressing Cas9-EGFP and 53BP1-mCherry is used for these experiments. A sub-micron 405 nm laser beam is directed to the targeted allele labeled by Cas9-EGFP, leading to activation of Cas9-EGFP/cgRNA only in that small region. The targeted allele is rapidly cleaved, while the activated uncaged Cas9-EGFP/cgRNA is diluted to very low concentration at equilibrium by the dominant population of inactive caged Cas9-EGFP/cgRNA. This inactive population also act as a competitive inhibitor by binding to and sequestering all possible target sites. We hypothesize that the combination of these factors disfavor cleavage of the non-targeted allele(s), putative off-target sites, and potentially the targeted allele again after repair has occurred. We test two experimental schemes: (1) Repetitive cleavage site (left): cgRNA targeting Ch3Rep is transfected or (2) Single cleavage site (right): cgRNA targeting *PPP1R2* is co-transfected with an 11-mer (inactive) sgRNA that only labels Ch3Rep for laser guidance.

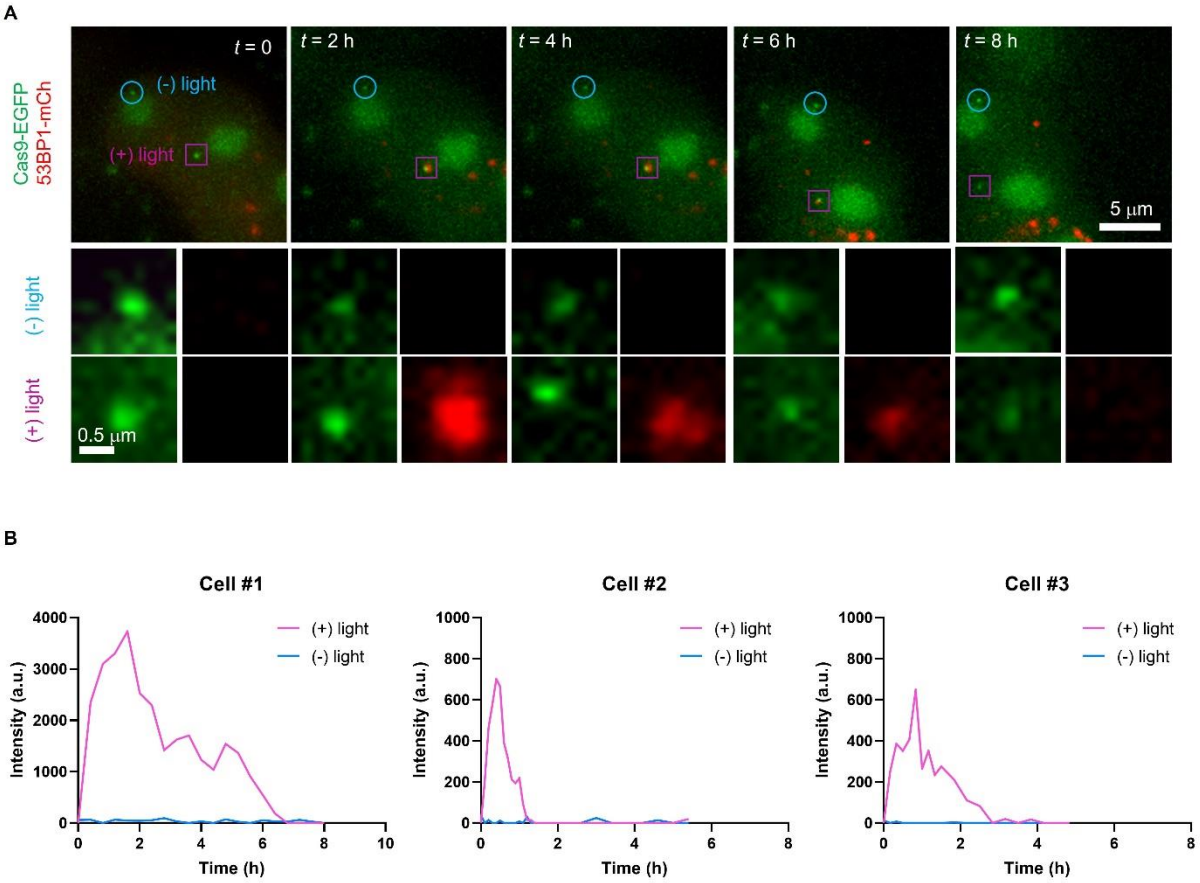


Fig. S25. Spatial control of Cas9 activation and 53BP1 recruitment at a single *PPP1R2* allele. (A) Representative images showing one cycle of 53BP1-mCherry recruitment at one *PPP1R2* allele (+ light, magenta square) but not on the other allele (- light, blue circle) in a single cell. (B) Fluorescence intensity traces of 53BP1-mCherry at either allele in three different cells. Cell #1 is the one featured in panel A. Only one 53BP1 cycle is expected here because after the initial single allele cleavage, the concentration of active Cas9-EGFP/cgRNA is so small compared to the inactive population that further cleavage activity is unlikely. See Figure S24 for a more detailed explanation.

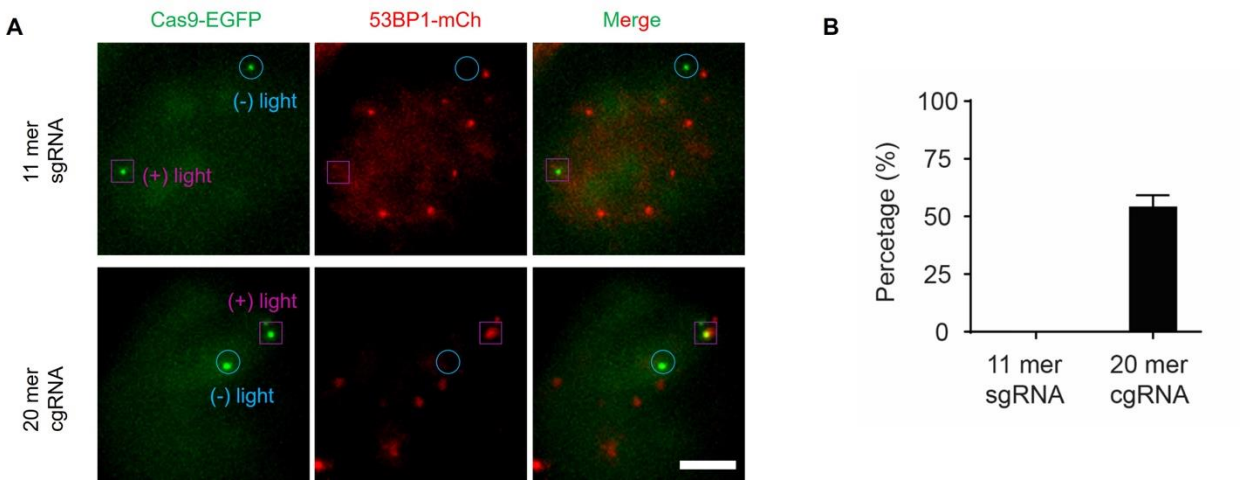


Fig. S26. Truncated sgRNA with 405nm focused laser did not lead to 53BP1-mCherry recruitment at Ch3Rep with single allele stimulation. One Ch3Rep allele was illuminated with the 405nm focused laser for (75 nW for 10 s) and appearance of 53BP1 foci was tracked for 1 hour after light illumination. No 53BP1-mCherry focus was observed when using 11-mer truncated sgRNA (85 cells, 3 biological replicates) versus over 50 % recruitment to one or both alleles using 20-mer light-inducible cgRNA (99 cells, 4 biological replicates). (A) Example of 53BP1 colocalization with Ch3Rep using 20-mer at the targeted allele, but not when using 11-mer. Scale bar, 5 µm. (B) Quantification of 53BP1 recruitment to either Ch3Rep allele for the 1 hour of tracking. This control experiment demonstrates that 53BP1-mCherry recruitment is dependent on Cas9 cleavage and not due to the light itself. Error bars represent standard deviation (n=2 biological replicates).

Table S1: crRNA and tracrRNA sequences

Name	**crRNA Sequences (5' to 3')** Green highlights dT-NPOM replacement; Red marks the RNA sequences hybridizing with target DNA
ACTB	GCUAUUCUCGCAGCUCACCAGUUUUAGAGCUAUGCUGUUUUG
IFT88	GUUACUAGACCUAUAGCUACGUUUUAGAGCUAUGCUGUUUUG
MYC	GUAAUUCCAGCGAGAGGCAGGUUUUAGAGCUAUGCUGUUUUG
PPP1R2	GACUUCCUCUAUGGUGGCGUGUUUUAGAGCUAUGCUGUUUUG
*VEGFA*site3	GGUGAGUGAGUGUGUGCGUGGUUUUAGAGCUAUGCUGUUUUG
Ch3Rep	UCCUCUGUAUGAUAUCACAGGUUUUAGAGCUAUGCUGUUUUG
Ch3Rep (11mer)	UGAUAUCACAGGUUUUAGAGCUAUGCUGUUUUG
Name	**tracrRNA sequences (5' to 3')**
tracrRNA	AGCAUAGCAAGUUAAAAUAAGGCUAGUCCGUUAUCAACUUGAA AAAGUGGCACCGAGUCGGUGCUUU

Note: All caged crRNAs were custom ordered from Biosynthesis Inc. TracrRNAs were purchased from IDT.

Table S2: dsDNA fragment sequences used in *in vitro* cleavage assays

Name	Sequences (5' to 3') Red marks WT/+1/-1 protospacer sequences. **+1** insertion is bold and underlined
ACTB WT	TGGCGGCCTAAGGACTCGGCGCGCCGGAAGTGGCCAGGGCGGGGGCGACTTCGGCTCACAGCGCGCCCGGC TATTCTCGCAGCTCACCATGGATGATGATATCGCCGCGCTCGTCGTCGACAACGGCTCCGGCATGTGCAAG GCCGGCTTCGCGGGCGACGATGCCCCCCGGGCCGTCTTCCCCTCCATCGTGGGGCGCCCCAGGCACCAGGT AGGGGAGCTGGCTGGGTGGGGCAGCCCCGGGAGCGGGCGGGAGGCAAGGGCGCTTTCTCTGCACAGGAGCC TCCCGGTTTCCGGGGTGGGGGCTGCGCCCGTGCTCAGGGCTTCTTGTCCTTTCCTTCCCAGGGCGTGATGG TGGGCATGGGTCAGAAGATTCCTATGTGGGCGACGAGGCCCAGAGCAAGAGAGGCATCCTCACCCTGAAG
ACTB +A	TGGCGGCCTAAGGACTCGGCGCGCCGGAAGTGGCCAGGGCGGGGGCGACTTCGGCTCACAGCGCGCCCGGC TATTCTCGCAGCTCA**A**CCATGGATGATGATATCGCCGCGCTCGTCGTCGACAACGGCTCCGGCATGTGCAA GGCCGGCTTCGCGGGCGACGATGCCCCCCGGGCCGTCTTCCCCTCCATCGTGGGGCGCCCCAGGCACCAGG TAGGGGAGCTGGCTGGGTGGGGCAGCCCCGGGAGCGGGCGGGAGGCAAGGGCGCTTTCTCTGCACAGGAGC CTCCCGGTTTCCGGGGTGGGGGCTGCGCCCGTGCTCAGGGCTTCTTGTCCTTTCCTTCCCAGGGCGTGATG GTGGGCATGGGTCAGAAGGATTCCTATGTGGGCGACGAGGCCCAGAGCAAGAGAGGCATCCTCACCCTGAA G
ACTB-pro +A	GGACTCACAACCACTCTCCTAGAGGCCAAGGTAGCCCTTGGGACTCAGGACCCTTCTGGTTGTCCCGA**A**GT GGGGCCTCAGAAGCTGGGTGACAAGTTGGGCCAGGAGAGATGGGGGTCAGTAGCAAGTTCAAGTTCAGGTC AAGTGGGGT
EZH1 +A	TCTTCCTCTCTTCCTTGGGCTTTTGAGAAAAGGGTGTCCACTCACAGGCTTCATTGACTGAACA**A**GGTTGG ACACGAAGCTTCTTCCATTCTTCATTGAGGATCTGGGTTTTTTCTTGAACCTTTGCAAAATTTGCCACATA CAAAGCCTAGC
MTA3 +T	CTATGATTTGAGCAGTGCCATTAGTGTCTTAGTACCACT**T**CGGAGGACCTGTTTTATGCAGAGATGAAATG GAGGTCTTGCCGTATGTCATTGAAGTAATGGTCAGCCTCTGAAGCTAGCTTATTTGAAGAGGCACTGGAA
ORC1 +T	TCCCAAACTCACCATCTTCGAACAACTCAAGCAATTTAGCAACATACGGGTTTTCATCATCATCCCCTTCA ATCAACACAAACTGTCCAATCTGGATGTGAATCT**T**CGGTGGAACAACCTTCTGTTTTCACACACATTTCTC TAGGAAGTAACAGAGAAGCACAT

Table S3: PCR primers for ddPCR

Name	Sequence (5' to 3')
*ACTB*_F1	TGGCGGCCTAAGGACTCG
*ACTB*_R1	GAAGCCGGCCTTGCACATG
*ACTB*_F2	CACAGGAGCCTCCCGGTTTC
*ACTB*_R2	CTTCAGGGTGAGGATGCCTCTC
*ACTB*_Probe1	/56-FAM/CGACCTCGG/ZEN/CTCACAGCGCGCC/3IABkFQ/
*ACTB*_Probe2	/5HEX/CTGCGCCCG/ZEN/TGCTCAGGGCTTCTTG/3IABkFQ/
*IFT88*_F1	CTCAGTCTGAATCCTGTTAAC
*IFT88*_R1	CCTAAAGTGAACTATTGTATGAG
*IFT88*_F2	GTGTCTATTGTTTGGCCTAGT
*IFT88*_R2	GTGAGAAGGAGACTCATTCT
*IFT88*_Probe1	/56-FAM/CTGCTAAAA/ZEN/TATCAAGCACGGCAG/3IABkFQ/
*IFT88*_Probe2	/5HEX/CTTATCGGC/ZEN/ACCTCAGATCGTTC/3IABkFQ/
*MYC*_F1	TTGGCGGGAAAAAGAACGG
*MYC*_R1	TATTCGCTCCGGATCTCCCT
*MYC*_F2	GCCAGCGGTCCGCAAC
*MYC*_R2	GAGAGCCTTTCAGAGAAGCGG
*MYC*_Probe1	/56-FAM/TCGGGGCTT/ZEN/TATCTAACTCGCTG/3IABkFQ/
*MYC*_Probe2	/5HEX/CACGAAACT/ZEN/TTGCCCATAGCAGC/3IABkFQ
*PPP1R2*_F1	GCCCATCAAGGGGATCTTGA
*PPP1R2*_R1	CTGGGGTCTGGGTAGGTAAC
*PPP1R2*_F2	CTCCTGCGCTGGAGCT
*PPP1R2*_R2	CAACTGCTGCCTCGGAAAC
*PPP1R2*_Probe1	/56-FAM/CTCTACGAC/ZEN/TTCCTCTATGGTGGCG/3IABkFQ/
*PPP1R2*_Probe2	/5HEX/CGTTGTGTC/ZEN/GTGACAACCGCTG/3IABkFQ/

Table S4: PCR primers for sanger sequencing

Name	Sequence (5' to 3')
*ACTB*_F	TGGCGGCCTAAGGACTCG
*ACTB*_R	CTTCAGGGTGAGGATGCCTCTC
*IFT88*_F	CTCAGTCTGAATCCTGTTAAC
*IFT88*_R	CACTTCTGAAACACTTTTCTTAC
*MYC*_F	TTGGCGGGAAAAAGAACGG
*MYC*_R	GAGAGCCTTTCAGAGAAGCGG
*PPP1R2*_F	GTTTCCGAGGCAGCAGTTG
*PPP1R2*_R	GCATGATAAACGTCATCGCCC

Table S5: Amplicon PCR primers for next generation sequencing

Name	Sequence (5' to 3')
NGS_*ACTB*_F	tcgtcggcagcgtcagatgtgtataagagacagTGGCGGCCTAAGGACTCG
NGS_*ACTB*_R	gtctcgtgggctcggagatgtgtataagagacagGAAGCCGGCCTTGCACATG
NGS_*IFT88*_F	tcgtcggcagcgtcagatgtgtataagagacagCTCAGTCTGAATCCTGTTAAC
NGS_*IFT88*_R	gtctcgtgggctcggagatgtgtataagagacagCCTAAAGTGAACTATTGTATGAG
NGS_*MYC*_F	tcgtcggcagcgtcagatgtgtataagagacagGGGATCGCGCTGAGTATAAA
NGS_*MYC*_R	gtctcgtgggctcggagatgtgtataagagacagTGGGCAAAGTTTCGTGGA
NGS_*PPP1R2*_F	tcgtcggcagcgtcagatgtgtataagagacagGCCCATCAAGGGGATCTTGA
NGS_*PPP1R2*_R	gtctcgtgggctcggagatgtgtataagagacagCTGGGGTCTGGGTAGGTAAC

Table S6: Dual-Indexing PCR primers for next generation sequencing

Name	**Sequence (5' to 3')** **Red** marks the i5 or i7 8 bp index sequence
NGS_Index_F1	AATGATACGGCGACCACCGAGATCTACAC**CTCTCTAT**TCGTCGGCAGCGTC
NGS_Index_F2	AATGATACGGCGACCACCGAGATCTACAC**TATCCTCT**TCGTCGGCAGCGTC
NGS_Index_F3	AATGATACGGCGACCACCGAGATCTACAC**GTAAGGAG**TCGTCGGCAGCGTC
NGS_Index_F4	AATGATACGGCGACCACCGAGATCTACAC**ACTGCATA**TCGTCGGCAGCGTC
NGS_Index_F5	AATGATACGGCGACCACCGAGATCTACAC**AAGGAGTA**TCGTCGGCAGCGTC
NGS_Index_F6	AATGATACGGCGACCACCGAGATCTACAC**CTAAGCCT**TCGTCGGCAGCGTC
NGS_Index_F7	AATGATACGGCGACCACCGAGATCTACAC**CGTCTAAT**TCGTCGGCAGCGTC
NGS_Index_F8	AATGATACGGCGACCACCGAGATCTACAC**TCTCTCCG**TCGTCGGCAGCGTC
NGS_Index_R1	CAAGCAGAAGACGGCATACGAGAT**TCGCCTTA**GTCTCGTGGGCTCGG
NGS_Index_R2	CAAGCAGAAGACGGCATACGAGAT**CTAGTACG**GTCTCGTGGGCTCGG
NGS_Index_R3	CAAGCAGAAGACGGCATACGAGAT**TTCTGCCT**GTCTCGTGGGCTCGG
NGS_Index_R4	CAAGCAGAAGACGGCATACGAGAT**GCTCAGGA**GTCTCGTGGGCTCGG
NGS_Index_R5	CAAGCAGAAGACGGCATACGAGAT**AGGAGTCC**GTCTCGTGGGCTCGG
NGS_Index_R6	CAAGCAGAAGACGGCATACGAGAT**CATGCCTA**GTCTCGTGGGCTCGG
NGS_Index_R7	CAAGCAGAAGACGGCATACGAGAT**GTAGAGAG**GTCTCGTGGGCTCGG
NGS_Index_R8	CAAGCAGAAGACGGCATACGAGAT**CAGCCTCG**GTCTCGTGGGCTCGG

Table S7: Oligos for preparing ChIP sequencing libraries

Name	Sequence (5' to 3') **Red** marks the i7 6 bp index sequence
MNase_F	/5Phos/GATCGGAAGAGCACACGTCT
MNase_R	ACACTCTTTCCCTACACGACGCTCTTCCGATC*T
PE_i5	AATGATACGGCGACCACCGAGATCTACACTCTTTCCCTACACGACGCTCTTCCGATC*T
PE_i701	CAAGCAGAAGACGGCATACGAGAT**CGTGAT**GTGACTGGAGTTCAGACGTGTGCTCTTCCGATC*T
PE_i702	CAAGCAGAAGACGGCATACGAGAT**ACATCG**GTGACTGGAGTTCAGACGTGTGCTCTTCCGATC*T
PE_i703	CAAGCAGAAGACGGCATACGAGAT**GCCTAA**GTGACTGGAGTTCAGACGTGTGCTCTTCCGATC*T
PE_i704	CAAGCAGAAGACGGCATACGAGAT**TGGTCA**GTGACTGGAGTTCAGACGTGTGCTCTTCCGATC*T
PE_i705	CAAGCAGAAGACGGCATACGAGAT**CACTGT**GTGACTGGAGTTCAGACGTGTGCTCTTCCGATC*T
PE_i706	CAAGCAGAAGACGGCATACGAGAT**ATTGGC**GTGACTGGAGTTCAGACGTGTGCTCTTCCGATC*T
PE_i707	CAAGCAGAAGACGGCATACGAGAT**GATCTG**GTGACTGGAGTTCAGACGTGTGCTCTTCCGATC*T
PE_i708	CAAGCAGAAGACGGCATACGAGAT**TCAAGT**GTGACTGGAGTTCAGACGTGTGCTCTTCCGATC*T
PE_i709	CAAGCAGAAGACGGCATACGAGAT**CTGATC**GTGACTGGAGTTCAGACGTGTGCTCTTCCGATC*T
PE_i710	CAAGCAGAAGACGGCATACGAGAT**AAGCTA**GTGACTGGAGTTCAGACGTGTGCTCTTCCGATC*T
PE_i711	CAAGCAGAAGACGGCATACGAGAT**GTAGCC**GTGACTGGAGTTCAGACGTGTGCTCTTCCGATC*T
PE_i712	CAAGCAGAAGACGGCATACGAGAT**TACAAG**GTGACTGGAGTTCAGACGTGTGCTCTTCCGATC*T
PE_i713	CAAGCAGAAGACGGCATACGAGAT**ATCAGT**GTGACTGGAGTTCAGACGTGTGCTCTTCCGATC*T
PE_i714	CAAGCAGAAGACGGCATACGAGAT**AGGAAT**GTGACTGGAGTTCAGACGTGTGCTCTTCCGATC*T
PE_i715	CAAGCAGAAGACGGCATACGAGAT**ATTCCG**GTGACTGGAGTTCAGACGTGTGCTCTTCCGATC*T
PE_i716	CAAGCAGAAGACGGCATACGAGAT**CCACTC**GTGACTGGAGTTCAGACGTGTGCTCTTCCGATC*T
PE_i717	CAAGCAGAAGACGGCATACGAGAT**CGATTA**GTGACTGGAGTTCAGACGTGTGCTCTTCCGATC*T
PE_i718	CAAGCAGAAGACGGCATACGAGAT**CTTCGA**GTGACTGGAGTTCAGACGTGTGCTCTTCCGATC*T
PE_i719	CAAGCAGAAGACGGCATACGAGAT**GAATGA**GTGACTGGAGTTCAGACGTGTGCTCTTCCGATC*T
PE_i720	CAAGCAGAAGACGGCATACGAGAT**GCGGAC**GTGACTGGAGTTCAGACGTGTGCTCTTCCGATC*T
PE_i721	CAAGCAGAAGACGGCATACGAGAT**GGAACT**GTGACTGGAGTTCAGACGTGTGCTCTTCCGATC*T
PE_i722	CAAGCAGAAGACGGCATACGAGAT**TAGTTG**GTGACTGGAGTTCAGACGTGTGCTCTTCCGATC*T
PE_i723	CAAGCAGAAGACGGCATACGAGAT**TCGGGA**GTGACTGGAGTTCAGACGTGTGCTCTTCCGATC*T
PE_i724	CAAGCAGAAGACGGCATACGAGAT**TCTGAG**GTGACTGGAGTTCAGACGTGTGCTCTTCCGATC*T

Table S8: Theoretical modeling and determination of DNA damage sensing and Cas9 target search in U-2 OS cells.

Gene	Initial arrival time (min)			Time gap (min)			Δ (min)
	$<T_1>$	τ_d	τ_s	$<T_{gap}>$	τ_d	τ_s	$B_0\tau_{s,\,avg}$
PPP1R2	49.1 ± 46.9	12.3 ± 2.2	42.7 ± 3.6	64.3 ± 58.0	8.0 ± 3.1	56.7 ± 5.8	7.5

Table S9: Summary of ChIP-seq sequencing data

Sample	Facility	Platform	Type	Reads	# samples
MRE11 timeseries	Sequencing core (MRB)	NextSeq500	2x36 High Output	430,769,462	12
γH2AX timeseries	Sequencing core (MRB)	NextSeq500	2x36 High Output	451,545,671	12
MRE11 DNA-PKi	Sequencing core (MRB)	NextSeq500	2x36 Mid Output	85,134,609	4

Caption for Table S10 (separate Excel file)

Table S10. Off-target detection using GUIDE-seq.

Captions for Movies S1 to S3

Movie S1 Cas9-induced 53BP1 recruitment to *PPP1R2*. Top row: at *t* = 0, U2OS cells expressing Cas9-EGFP and 53BP1-mCherry were globally stimulated using a flashlight (365 nm, 40 mW/cm2, 30 s). The formation of 53BP1-mCherry foci was observed at two distinct loci (highlighted by the magenta square and cyan circle). The time lapse movie was streamed at an interval of 3 min for 8 h. Green: Cas9-EGFP, Red: 53BP1-mCherry. Scale Bar: 5 µm. Bottom row: Fluorescence intensity traces of 53BP1-mCherry displaying the DDR at two corresponding alleles in real-time.

Movie S2: Cas9-induced 53BP1 recruitment to Ch3Rep at a single allele. Top row: Recruitment of 53BP1-mCherry to a single Ch3Rep allele in U2OS cells. The specific single allele was guided by imaging of Cas9-EGFP focus and stimulated using a focused laser (405 nm, 78 nW, 10 s, stimulation region highlighted by the magenta square). The time lapse movie was streamed at an interval of 1 min for 1 h. Green: Cas9-EGFP, Red: 53BP1-mCherry. Scale Bar: 5 µm. Bottom row: Fluorescence intensity traces of 53BP1-mCherry showing only DDR at the stimulated allele (magenta square) but not the non-stimulated allele (cyan circle).

Movie S3: Cas9-induced 53BP1 recruitment to *PPP1R2* at a single allele. Top row: Recruitment of 53BP1-mCherry to a single *PPP1R2* allele in U2OS cells. The specific single allele was guided by imaging of Cas9-EGFP focus and stimulated using a focused laser (405 nm, 65 µW, 100 ms, stimulation region highlighted by the magenta square). The time lapse movie was streamed at an interval of 5 min for 8 h. Green: Cas9-EGFP, Red: 53BP1-mCherry. Scale Bar: 5 µm. Bottom row: Fluorescence intensity traces of 53BP1-mCherry showing only DDR at the stimulated allele (magenta square) but not the non-stimulated allele (cyan circle).

References and Notes

1. G. J. Knott, J. A. Doudna, CRISPR-Cas guides the future of genetic engineering. *Science* **361**, 866–869 (2018). doi:10.1126/science.aat5011 Medline

2. S. E. Polo, S. P. Jackson, Dynamics of DNA damage response proteins at DNA breaks: A focus on protein modifications. *Genes Dev.* **25**, 409–433 (2011). doi:10.1101/gad.2021311 Medline

3. M. van Overbeek, D. Capurso, M. M. Carter, M. S. Thompson, E. Frias, C. Russ, J. S. Reece-Hoyes, C. Nye, S. Gradia, B. Vidal, J. Zheng, G. R. Hoffman, C. K. Fuller, A. P. May, DNA repair profiling reveals nonrandom outcomes at Cas9-mediated breaks. *Mol. Cell* **63**, 633–646 (2016). doi:10.1016/j.molcel.2016.06.037 Medline

4. B. R. Lemos, A. C. Kaplan, J. E. Bae, A. E. Ferrazzoli, J. Kuo, R. P. Anand, D. P. Waterman, J. E. Haber, CRISPR/Cas9 cleavages in budding yeast reveal templated insertions and strand-specific insertion/deletion profiles. *Proc. Natl. Acad. Sci. U.S.A.* **115**, E2040–E2047 (2018). doi:10.1073/pnas.1716855115 Medline

5. S. Lin, B. T. Staahl, R. K. Alla, J. A. Doudna, Enhanced homology-directed human genome engineering by controlled timing of CRISPR/Cas9 delivery. *eLife* **3**, e04766 (2014). doi:10.7554/eLife.04766 Medline

6. E. M. Kallimasioti-Pazi, K. Thelakkad Chathoth, G. C. Taylor, A. Meynert, T. Ballinger, M. J. E. Kelder, S. Lalevée, I. Sanli, R. Feil, A. J. Wood, Heterochromatin delays CRISPR-Cas9 mutagenesis but does not influence the outcome of mutagenic DNA repair. *PLOS Biol.* **16**, e2005595 (2018). doi:10.1371/journal.pbio.2005595 Medline

7. L. E. Dow, J. Fisher, K. P. O'Rourke, A. Muley, E. R. Kastenhuber, G. Livshits, D. F. Tschaharganeh, N. D. Socci, S. W. Lowe, Inducible in vivo genome editing with CRISPR-Cas9. *Nat. Biotechnol.* **33**, 390–394 (2015). doi:10.1038/nbt.3155 Medline

8. B. Zetsche, S. E. Volz, F. Zhang, A split-Cas9 architecture for inducible genome editing and transcription modulation. *Nat. Biotechnol.* **33**, 139–142 (2015). doi:10.1038/nbt.3149 Medline

9. Y. Nihongaki, F. Kawano, T. Nakajima, M. Sato, Photoactivatable CRISPR-Cas9 for optogenetic genome editing. *Nat. Biotechnol.* **33**, 755–760 (2015). doi:10.1038/nbt.3245 Medline

10. J. Hemphill, E. K. Borchardt, K. Brown, A. Asokan, A. Deiters, Optical control of CRISPR/Cas9 gene editing. *J. Am. Chem. Soc.* **137**, 5642–5645 (2015). doi:10.1021/ja512664v Medline

11. P. K. Jain, V. Ramanan, A. G. Schepers, N. S. Dalvie, A. Panda, H. E. Fleming, S. N. Bhatia, Development of light-activated CRISPR using guide RNAs with photocleavable protectors. *Angew. Chem. Int. Ed.* **55**, 12440–12444 (2016). doi:10.1002/anie.201606123 Medline

12. J. E. Dahlman, O. O. Abudayyeh, J. Joung, J. S. Gootenberg, F. Zhang, S. Konermann, Orthogonal gene knockout and activation with a catalytically active Cas9 nuclease. *Nat. Biotechnol.* **33**, 1159–1161 (2015). doi:10.1038/nbt.3390 Medline

13. D. Singh, S. H. Sternberg, J. Fei, J. A. Doudna, T. Ha, Real-time observation of DNA recognition and rejection by the RNA-guided endonuclease Cas9. *Nat. Commun.* **7**, 12778 (2016). doi:10.1038/ncomms12778 Medline

14. D. Singh, Y. Wang, J. Mallon, O. Yang, J. Fei, A. Poddar, D. Ceylan, S. Bailey, T. Ha, Mechanisms of improved specificity of engineered Cas9s revealed by single-molecule FRET analysis. *Nat. Struct. Mol. Biol.* **25**, 347–354 (2018). doi:10.1038/s41594-018-0051-7 Medline

15. S. H. Sternberg, B. LaFrance, M. Kaplan, J. A. Doudna, Conformational control of DNA target cleavage by CRISPR-Cas9. *Nature* **527**, 110–113 (2015). doi:10.1038/nature15544 Medline

16. H. Lusic, D. D. Young, M. O. Lively, A. Deiters, Photochemical DNA activation. *Org. Lett.* **9**, 1903–1906 (2007). doi:10.1021/ol070455u Medline

17. J. C. Rose, J. J. Stephany, W. J. Valente, B. M. Trevillian, H. V. Dang, J. H. Bielas, D. J. Maly, D. M. Fowler, Rapidly inducible Cas9 and DSB-ddPCR to probe editing kinetics. *Nat. Methods* **14**, 891–896 (2017). doi:10.1038/nmeth.4368 Medline

18. B. Wienert, S. K. Wyman, C. D. Richardson, C. D. Yeh, P. Akcakaya, M. J. Porritt, M. Morlock, J. T. Vu, K. R. Kazane, H. L. Watry, L. M. Judge, B. R. Conklin, M. Maresca, J. E. Corn, Unbiased detection of CRISPR off-targets in vivo using DISCOVER-Seq. *Science* **364**, 286–289 (2019). Medline

19. S. Q. Tsai, Z. Zheng, N. T. Nguyen, M. Liebers, V. V. Topkar, V. Thapar, N. Wyvekens, C. Khayter, A. J. Iafrate, L. P. Le, M. J. Aryee, J. K. Joung, GUIDE-seq enables genome-wide profiling of off-target cleavage by CRISPR-Cas nucleases. *Nat. Biotechnol.* **33**, 187–197 (2015). doi:10.1038/nbt.3117 Medline

20. H. Yin, C. Q. Song, S. Suresh, S. Y. Kwan, Q. Wu, S. Walsh, J. Ding, R. L. Bogorad, L. J. Zhu, S. A. Wolfe, V. Koteliansky, W. Xue, R. Langer, D. G. Anderson, Partial DNA-guided Cas9 enables genome editing with reduced off-target activity. *Nat. Chem. Biol.* **14**, 311–316 (2018). doi:10.1038/nchembio.2559 Medline

21. E. K. Brinkman, T. Chen, M. de Haas, H. A. Holland, W. Akhtar, B. van Steensel, Kinetics and fidelity of the repair of Cas9-induced double-strand DNA breaks. *Mol. Cell* **70**, 801–813.e6 (2018). doi:10.1016/j.molcel.2018.04.016 Medline

22. R. Aleksandrov, A. Dotchev, I. Poser, D. Krastev, G. Georgiev, G. Panova, Y. Babukov, G. Danovski, T. Dyankova, L. Hubatsch, A. Ivanova, A. Atemin, M. N. Nedelcheva-Veleva, S. Hasse, M. Sarov, F. Buchholz, A. A. Hyman, S. W. Grill, S. S. Stoynov, Protein dynamics in complex DNA lesions. *Mol. Cell* **69**, 1046–1061.e5 (2018). doi:10.1016/j.molcel.2018.02.016 Medline

23. T. Clouaire, V. Rocher, A. Lashgari, C. Arnould, M. Aguirrebengoa, A. Biernacka, M. Skrzypczak, F. Aymard, B. Fongang, N. Dojer, J. S. Iacovoni, M. Rowicka, K. Ginalski, J. Côté, G. Legube, Comprehensive mapping of histone modifications at DNA double-strand breaks deciphers repair pathway chromatin signatures. *Mol. Cell* **72**, 250–262.e6 (2018). doi:10.1016/j.molcel.2018.08.020 Medline

24. B. Chen, L. A. Gilbert, B. A. Cimini, J. Schnitzbauer, W. Zhang, G. W. Li, J. Park, E. H. Blackburn, J. S. Weissman, L. S. Qi, B. Huang, Dynamic imaging of genomic loci in

living human cells by an optimized CRISPR/Cas system. *Cell* **155**, 1479–1491 (2013). doi:10.1016/j.cell.2013.12.001 Medline

25. H. Ma, L. C. Tu, A. Naseri, M. Huisman, S. Zhang, D. Grunwald, T. Pederson, Multiplexed labeling of genomic loci with dCas9 and engineered sgRNAs using CRISPRainbow. *Nat. Biotechnol.* **34**, 528–530 (2016). doi:10.1038/nbt.3526 Medline

26. H. Wang, M. Nakamura, T. R. Abbott, D. Zhao, K. Luo, C. Yu, C. M. Nguyen, A. Lo, T. P. Daley, M. La Russa, Y. Liu, L. S. Qi, CRISPR-mediated live imaging of genome editing and transcription. *Science* **365**, 1301–1305 (2019). doi:10.1126/science.aax7852 Medline

27. N. Dimitrova, Y. C. M. Chen, D. L. Spector, T. de Lange, 53BP1 promotes non-homologous end joining of telomeres by increasing chromatin mobility. *Nature* **456**, 524–528 (2008). doi:10.1038/nature07433 Medline

28. D. Paquet, D. Kwart, A. Chen, A. Sproul, S. Jacob, S. Teo, K. M. Olsen, A. Gregg, S. Noggle, M. Tessier-Lavigne, Efficient introduction of specific homozygous and heterozygous mutations using CRISPR/Cas9. *Nature* **533**, 125–129 (2016). doi:10.1038/nature17664 Medline

29. K. Jaqaman, D. Loerke, M. Mettlen, H. Kuwata, S. Grinstein, S. L. Schmid, G. Danuser, Robust single-particle tracking in live-cell time-lapse sequences. *Nat. Methods* **5**, 695–702 (2008). doi:10.1038/nmeth.1237 Medline

30. C. McQuin, A. Goodman, V. Chernyshev, L. Kamentsky, B. A. Cimini, K. W. Karhohs, M. Doan, L. Ding, S. M. Rafelski, D. Thirstrup, W. Wiegraebe, S. Singh, T. Becker, J. C. Caicedo, A. E. Carpenter, CellProfiler 3.0: Next-generation image processing for biology. *PLOS Biol.* **16**, e2005970 (2018). doi:10.1371/journal.pbio.2005970 Medline

31. T. Mamo, A. C. Mladek, K. L. Shogren, C. Gustafson, S. K. Gupta, S. M. Riester, A. Maran, M. Galindo, A. J. van Wijnen, J. N. Sarkaria, M. J. Yaszemski, Inhibiting DNA-PK$_{CS}$ radiosensitizes human osteosarcoma cells. *Biochem. Biophys. Res. Commun.* **486**, 307–313 (2017). doi:10.1016/j.bbrc.2017.03.033 Medline

32. N. Uematsu, E. Weterings, K. Yano, K. Morotomi-Yano, B. Jakob, G. Taucher-Scholz, P. O. Mari, D. C. van Gent, B. P. C. Chen, D. J. Chen, Autophosphorylation of DNA-PKCS regulates its dynamics at DNA double-strand breaks. *J. Cell Biol.* **177**, 219–229 (2007). doi:10.1083/jcb.200608077 Medline

33. R. Perrault, H. Wang, M. Wang, B. Rosidi, G. Iliakis, Backup pathways of NHEJ are suppressed by DNA-PK. *J. Cell. Biochem.* **92**, 781–794 (2004). doi:10.1002/jcb.20104 Medline

34. Q. Ding, Y. V. R. Reddy, W. Wang, T. Woods, P. Douglas, D. A. Ramsden, S. P. Lees-Miller, K. Meek, Autophosphorylation of the catalytic subunit of the DNA-dependent protein kinase is required for efficient end processing during DNA double-strand break repair. *Mol. Cell. Biol.* **23**, 5836–5848 (2003). doi:10.1128/MCB.23.16.5836-5848.2003 Medline

35. A. M. Chakrabarti, T. Henser-Brownhill, J. Monserrat, A. R. Poetsch, N. M. Luscombe, P. Scaffidi, Target-Specific Precision of CRISPR-Mediated Genome Editing. *Mol. Cell* **73**, 699–713.e6 (2019). doi:10.1016/j.molcel.2018.11.031 Medline

36. J. S. Iacovoni, P. Caron, I. Lassadi, E. Nicolas, L. Massip, D. Trouche, G. Legube, High-resolution profiling of gammaH2AX around DNA double strand breaks in the mammalian genome. *EMBO J.* **29**, 1446–1457 (2010). doi:10.1038/emboj.2010.38 Medline

37. J. A. Kim, M. Kruhlak, F. Dotiwala, A. Nussenzweig, J. E. Haber, Heterochromatin is refractory to γ-H2AX modification in yeast and mammals. *J. Cell Biol.* **178**, 209–218 (2007). doi:10.1083/jcb.200612031 Medline

38. R. Shroff, A. Arbel-Eden, D. Pilch, G. Ira, W. M. Bonner, J. H. Petrini, J. E. Haber, M. Lichten, Distribution and dynamics of chromatin modification induced by a defined DNA double-strand break. *Curr. Biol.* **14**, 1703–1711 (2004). doi:10.1016/j.cub.2004.09.047 Medline